Defective phagocytic function of induced microglia-like cells is correlated with rapid progression of sporadic ALS

Min-Young Noh
Hanyang University College of Medicine
Min-Soo Kwon
CHA University
Ki-WooK Oh
Hanyang University College of Medicine
Minyeop Nahm
Hanyang University College of Medicine
Jinseok Park
Hanyang University College of Medicine
Young-Eun Kim
Hanyang University College of Medicine
Chang-Seok Ki
Green Cross Corporation
Hee Kyung Jin
Kyungpook National University
Jae-sung Bae
Kyungpook National University School of Medicine
Seung Hyun Kim (kimsh1@hanyang.ac.kr)
Hanyang University College of Medicine https://orcid.org/0000-0001-9644-9598

Research article

Keywords: Amyotrophic lateral sclerosis, Microglia, NCKAP1, miRNA-214, Phagocytosis

Posted Date: May 23rd, 2020

DOI: https://doi.org/10.21203/rs.3.rs-29976/v1

Abstract

Background: Microglia play a key role in determining the progression of amyotrophic lateral sclerosis (ALS), yet their precise role in ALS has not been identified in humans. The objective of this study was to identify the functional characteristics of microglia and related factors in patients with sporadic ALS that is rapidly progressing.

Methods: After confirming that microglia-like cells (iMGs) induced by human monocytes could recapitulate the main signatures of brain microglia, serial comparative studies were conducted to delineate functional differences in iMGs from patients with slowly progressive ALS [ALS(S), n = 14] versus rapidly progressive ALS [ALS(R), n = 15].

Results: Despite an absence of significant differences in the expression of microglial homeostatic genes, ALS(R)-iMGs preferentially showed defective phagocytosis and an exaggerated pro-inflammatory response to LPS stimuli compared to ALS(S)-iMGs. Transcriptome analysis revealed that the perturbed phagocytosis seen in ALS(R)-iMGs was closely associated with decreased NCKAP1 (NCK-associated protein 1)-mediated abnormal actin polymerization. NCKAP1 overexpression was sufficient to rescue impaired phagocytosis in ALS(R)-iMGs. To leverage our findings and identify biological markers of rapidly progressing ALS, we measured plasma miRNA-214-3p (negative regulator targeting NCKAP1) levels. Post-hoc analysis indicated that decreased NCKAP1 expression in iMGs and a concomitant increase in plasma miRNA-214-3p levels was correlated with rapid progression of ALS.

Interpretation: Our data suggest that microglial NCKAP1 may be an alternative therapeutic target in rapidly progressive sporadic ALS. In addition, miRNA-214-3p levels could be a serological biomarker for predicting the speed of disease progression.

Background

Amyotrophic lateral sclerosis (ALS) is a fatal neurodegenerative disease characterized by loss of motor neurons and inflammation in the motor neural axis, including the primary motor cortex, brainstem, and spinal cord. It results in muscle weakness, wasting, respiratory paralysis, and, ultimately, death within 3 – 5 years [1].

The clinical progression of ALS is highly variable. Microglial cells play a crucial role in determining the clinical progression of ALS [2]. The dual roles of microglia (i.e., protective or toxic effect according to disease stage) have been thoroughly described in an *SOD1* mutant mouse model [3, 4]. However, most ALS cases are sporadic (sALS) and results from the SOD1 mutant mouse model are inadequate to describe microglial function in sporadic ALS. Moreover, reactive microglial phagocytosis exhibits a neuroprotective effect rather than exacerbating motor neuron death in a model of *TDP-43* proteinopathy, the most common pathology found in sALS, in contrast to a SOD1 mutant mouse model [5, 6]. Furthermore, the results of previous clinical trials that looked at the use of anti-inflammatory drugs in ALS suggest that complete suppression of microglial function seems to be irrelevant to optimal control of the

neuro-inflammatory process [7, 8]. These findings suggest that the nature of neuroinflammation is not uniform across pathological conditions. It appears to be contingent on the type of stimulus, its duration, and the regions involved [9]. In addition, not only non-neuronal cells such as microglia [10] and astrocytes [11], but also peripheral monocytes contribute to the inflammatory process and immune dysfunction in ALS [2, 12]. Recent evidence suggests that peripheral monocytes contribute to the speed of ALS progression [13] and that modulating their inflammatory activity can ameliorate murine ALS [14, 15]. These findings provide important insights into the process of neuroinflammation, which is induced by a complex integrated form not jus a separated manner.

Recent studies have shown that microglia can be divided into diverse microglial subtypes, such as disease-associated microglia (DAM) and microglial neurodegenerative phenotype (MGnD), depending on the surrounding inflammatory milieu [16-18]. Despite the importance of understanding the role of each microglial subpopulation based on single-cell assays in ALS, it is practically impossible to assess the overall functional status of *in situ* microglia and other cells that concomitantly participate in the complex inflammatory process in living ALS patients based off of single-cell assays. Although induced pluripotent stem cells (iPSCs) and a co-cultured model have been used to study microglia [19-21], iPSC-derived microglia-like cells have drawbacks; for example, they do not reflect current pathological status due to rejuvenation [22]. In addition, they require intricate procedures with low reprogramming efficiency and take a long time to grow and study [23-25]. On the other hand, microglia-like cells induced from monocytes (iMGs) have an advantage in that they mirror the current pathophysiological state of CNS phagocytes [24, 26, 27]. Although they are not identical to yolk sac-derived microglia, iMGs can be used as a model system to interpret human microglial pathology in living patients, at least to some extent [23, 26-28].

Our hypothesis is that microglia-related inflammatory processes and their main functions differ according to the speed of progression of ALS. After validating the iMG model in healthy donors, the reliability of our iMG protocol was confirmed again by demonstrating that iMGs share major subsets of genes that are related to innate immune functions of microglia in living ALS patients. After that, serial comprehensive comparative studies delineating the molecular and functional differences of iMGs, including the signature gene expression pattern of microglia, morphology, and phagocytic function, were conducted in slowly [ALS(S)] and rapidly [ALS(R)] progressing ALS patients and healthy controls. Our approach identified unique phagocytic dysfunction in ALS(R)-iMGs. Finally, we identified a molecular target associated with the defective phagocytic function of iMGs and a possible serologic biomarker that can be used to predict the speed of progression of sALS.

Methods

Study design

The aim of this study was to find key factors related to microglial functional differences according to ALS progression speed using a microglia-like cell model (iMGs) as a translational research tool. First, the iMG

model was shown to exhibit the signature gene patterns of brain microglia and the innate functions of microglia in healthy donors. To further validate the model, we compared iMGs to brain microglia that were obtained from the same ALS patient. Thereafter, we conducted a systematic comparative analysis to delineate the different natures of iMGs in ALS patients according to speed of clinical progression. We enrolled two distinct sporadic ALS patient groups dichotomized by clinical progression speed: one group with slowly progressing ALS [ALS(S), n = 14] and one group with rapidly progressing ALS [ALS(R), n = 15] according to the revised El Escorial criteria between September 2015 and July 2017. Second, we endeavored to identify target molecule(s) related to the functional properties of microglia that are present only in ALS(R)-iMGs. To do this, we compared transcriptome data between ALS(R)-iMGs and ALS(S)-iMGs. Subsequently, we conducted functional studies on an identified target molecule. Finally, we found a clinically applicable serologic biomarker related to activity of the target molecule that is well correlated with both levels of the target molecule and speed of progression of ALS.

Participants and Samples

We enrolled five healthy volunteers and twenty-nine patients with sporadic ALS (14 patients with slow progression and 15 patients with rapid progression) according to the revised El Escorial criteria [29] between September 2015 and July 2017. Patients with clinically definite, clinically probable, clinically probable with laboratory-supported, or possible sALS were recruited for this study. None of the participants had any evidence of recent infectious or inflammatory diseases. Individual medical records were reviewed to obtain clinical characteristics such as age, sex, family history of ALS, region of symptom onset, ALS functional rating scale-revised (ALSFRS-R) score [29], and changing pattern of ALSFRS-R score reflecting the speed of progression of ALS. The progression rate was defined as delta FS [30], (i.e., (48 - ALSFRS-R score at the time of diagnosis)/(duration from onset to diagnosis in months)). In order to enroll only participants who exhibited extremely slow or extremely rapid clinical progression, the sALS patients were categorized by using Hanyang MND registry as follows: The mean value was 0.83±0.81, slowly progressive ALS = delta FS $\leq$ 0.36, and rapidly progressive ALS = delta FS > 1.0. The difference between delta FS value (from onset to diagnosis vs. from onset to at the time of blood sampling) was not significant in both groups. The clinical and genetic characteristics of the participants are presented in Additional file 1: Table S1. Schematic outlines of the serial studies that are described in the Methods and Results sections are summarized in Additional file 2: Figure S1. Blood samples were obtained for generation of iMGs and *post-hoc* analysis of biomarkers, including inflammatory cytokines and microRNAs, after obtaining informed consent from each patient with sALS and matched controls comparable in age and sex at the ALS clinic, Hanyang University Hospital, Seoul, Republic of Korea. This study was conducted in accordance with the World Medical Association's Declaration of Helsinki. It was approved by the Ethics Committee of Hanyang University (HYUH IRB 2013-06-012 and 2017-01-043).

Genetic analysis

Genomic DNA was extracted from peripheral blood leukocytes using a standard procedure. Next-generation sequencing (NGS) was performed with SureSelect Human All Exon V5 (SureSelect; Agilent Technologies, Santa Clara, CA) on a NextSeq500 platform (Illumina, Inc.). Alignment of sequence reads, indexing of a reference genome (GRCh37/hg19), and variant calling were performed with a pipeline based on GATK Best Practices. Variants with allele frequencies > 0.01 identified in the Genome Aggregation Database (http://gnomad.broadinstitute.org/) were filtered out. Variants found in 1,100 ethnically-matched controls from the Korean Reference Genome Database (http://152.99.75.168/KRGDB/) were also filtered out. Next, 46 genes related to frontotemporal dementia (FTD), ALS, and other dementias were screened for pathogenic or likely pathogenic variants (Additional file 1: Table S1 and Additional file 3: Table S2). These variants were classified according to the guidelines of the American College of Medical Genetics and Genomics (ACMG) and the Association for Molecular Pathology (AMP). APOE genotype was also analyzed using whole-exon sequencing data (Additional file 1: Table S1).

Establishment of induced microglia-like cells (iMGs) from human peripheral blood

iMG cells were established based on a method previously published by Ohganani [27]. Briefly, peripheral blood was collected from healthy adult volunteers and ALS patients using a heparinized tube. PBMCs were isolated by density gradient centrifugation using Ficoll (GE Healthcare), according to our previous study [31]. The cells were resuspended in RPMI-1640 (Gibco, Waltham, MA) containing 10% FBS (Gibco) and 1% antibiotic/antimycotic (Invitrogen, Carlsbad, CA). PBMCs were plated in culture chambers at a density of 500,000 cells/ml and cultured overnight under standard culture conditions (37°C, 5% CO_2). On the next day, the medium was carefully aspirated and adherent cells (monocytes) were cultured in RPMI-1640 Glutamax (Gibco) supplemented with 1% antibiotic/antimycotic, recombinant human granulocyte-macrophage colony-stimulating factor (GM-CSF) (10 ng/ml; R&D Systems, Minneapolis, MN), and recombinant human interleukin-34 (IL-34) (100 ng/ml; R&D Systems) to develop iMG cells. After 14 days, the plates were washed thoroughly to remove any unbound cells. Fresh medium with GM-CSF and IL-34 was then added. Cells were harvested or used for functional assays for up to 21 days (7 additional days). For microglia stimulation, cells were treated with 100 ng/ml lipopolysaccharide (LPS, Sigma-Aldrich, St. Louis, MO) for 18 h, 40 ng/ml IL-4 (Peprotech, Rocky Hill, NJ) for 72 h, or 2 nM dexamethasone (Sigma Aldrich) for 72 h [32].

Cell morphology

Morphological changes of microglia-like cells were examined using a phase-contrast microscope (TS100-F; Nikon Instech, Tokyo, Japan). Images were captured with a DS-Vi1 digital camera (Nikon Instech) and a DS-L3 control unit (Nikon Instech).

Flow cytometry

Fluorochrome-conjugated monoclonal antibodies specific for human CD11b (APCVio770; Miltenyi Biotec, Gladbach, Germany) and CD45 (PE; Miltenyi Biotec) were used for iMGs phenotyping. The cells were washed with MACS buffer (Miltenyi Biotec) and incubated at 4°C for 5 min in FcR-blocking reagent (Miltenyi Biotec). The cell suspension was incubated with antibodies for 30 min at 4°C, washed with calcium-magnesium-free phosphate-buffered saline (PBS), resuspended, and fixed with 1% paraformaldehyde (Wako, Osaka, Japan) in PBS. The expression ratio of CD11b to CD45 was calculated from the fluorescence intensity of each fluorochrome. All data were collected with a FACS Canto II flow cytometer (BD Biosciences) and analyzed with FACS Diva and Flow Jo software (BD Biosciences).

Immunocytochemistry

The cells were fixed with 4% paraformaldehyde and permeabilized with 0.3% Triton X-100 for 5 min, then blocked with 1% bovine serum albumin (BSA) in PBS for 1 hour. Then, the samples were incubated with primary antibodies overnight at 4°C and labeled with secondary antibodies for 30 min at room temperature. The following primary antibodies were used in this study: Rabbit anti-CX3CR1 (Abcam, ab8021, 1:200), mouse anti-CCR2 (R&D Systems, MAB150, 1:200), rabbit anti-P2RY12 (Abcam, ab140862, 1:200), rabbit anti-P2RY12 (antibodies-online, ABIN1387659, 1:200), mouse anti-IBA1 (Abcam, ab15690, 1:200), rabbit anti-IBA1 (Wako, 019-19741, 1:200), rabbit anti-TMEM119 (Abcam, ab185337, 1:200), goat anti-TMEM119 (Santa Cruz, SC-244341, 1:200), mouse anti-PU.1/Spi1 (Abcam, ab88082, 1:200), rabbit anti-PU.1/Spi1 (Cell Signaling Technology, 2266, 1:100), rabbit anti-NCKAP1 (Novus Biologicals, NBP1-83269, 1:200), mouse anti-WAVE (Santa Cruz, sc-373889, 1:200), and mouse anti-ABI (Santa Cruz, sc-398554, 1:200). Alexa 488-, Alexa 546-, or Alexa 647-conjugated secondary antibodies (Invitrogen) were used for detection. To stain actin filaments, cells were incubated with fluorescent phalloidin (Molecular Probes, 1: 1,000 dilution) for 45 min with secondary antibodies. The samples were mounted in SlowFade antifade medium (Invitrogen). Images were acquired with a confocal microscope (TCS SP5, Leica, Wetzlar, Germany). Three-dimensional reconstructions of randomly selected iMG cells (IBA-1-positive) were generated using Imaris software (Bitplane, Zurich, Switzerland). Morphometric analysis of each reconstructed cell was then performed by two blinded researchers after determining dendrite length, number of segments, branch point, terminal point, and surface volume [33].

Quantitative real time-polymerase chain reaction (qRT-PCR)

Total RNA was extracted using Trizol reagent (Invitrogen) and evaluated using a NanoDrop 2000 spectrophotometer (Thermo Scientific, ND-2000). cDNA was synthesized using an EcoDryTM cDNA kit (Clontech, CA, USA). To assess the microglia signature in HC-iMGs, we analyzed the gene expression

levels of *P2RY12* (Qiagen, Germany, PPH02545B), *OLFML3* (PPH07681A), *OLFML3* (PPH07681A), *TGFBR1* (PPH00237C), *TMEM119* (PPH21875A), *TREM2* (PPH06065E), and *GAPDH* (PPH00150F). To evaluate gene expression patterns in iMG cells after treatment with LPS, IL-4, dexamethasone, or during phagocytosis, we analyzed *HLA-DR* (PPH00857F), *CD45* (PPH01510C), *TNF-α* (PPH00341F), *CCR7* (PPH00617A), *CCL18* (PPH00574C), and *CD200R* (PPH16717A) mRNA levels. To assess microglia signature and senescence in ALS(S) and ALS(R)-iMGs cells, we analyzed *GPR34* (PPH08814A), *MERTK* (PPH 16600A), *CSF1R* (PPH00191F), *HEXB* (PPH09801A), *p21* (NM_000389, F–CGAAGTCAGTTCCTTGTGGAG, R-CATGGGTTCTGACGGACAT), and *p16* (PPH00207C) mRNA levels. To confirm the transcriptome analysis results, *NCKAP1* (PPH15666A), *VAV3* (PPH0150E), *MYO10* (PPH09689A), *FYN* (PPH15624A), *ARPC1A* (PPH16239A), *SLC11A1* (PPH05732F), *MFGE8* (PPH07218A), *ANXA11* (PPH06949A), *WAS* (PPH07123A), *PTX3* (PPH01105A), *CD36* (PPH01456A), *FCGR2B* (PPH02368C), *GAS6* (PPH00025F), *TYROBP* (PPH07729A), and *TREM2* (PPH06065E) were analyzed. To examine alterations in the expression of pro- and anti-inflammatory cytokines after LPS stimulation (100 ng/ml for 18 h), we analyzed *TNF-α* (PPH00341F), *IL-6* (PPH00560C), *IL-1β* (PPH00171C), *TGF-β* (PPH00524B), *IL-10* (PPH00572C), *NF-κB-p50* (PPH00204F), and *NF-κB-p65* (PPH01812B) mRNA levels. cDNA was amplified using Power SYBR Green PCR Master Mix with primers on an Applied Biosystems Step One Plus^{TM} system (Life Technologies) at 95°C for 10 min, followed by 40 cycles of 15 s at 95°C and 1 min at 60°C. A melting curve was generated to examine the specificity of amplification. Relative quantity (RQ) levels were calculated with the $2^{-\Delta\Delta Ct}$ method using *GAPDH* as an internal standard control. The reported results are based on three independent experiments carried out on separate batches of cells.

Phagocytosis assay

To quantify phagocytosis in iMGs, iMGs that had been optimally cultured for 21 days were treated with 4 μl red fluorescent latex beads for 24 h at 37°C. Phagocytic activity was halted with the addition of 2 ml ice-cold PBS. The cells were washed twice with ice-cold PBS, fixed, stained with a microglial marker (IBA-1 or P2RY12), and counterstained with DAPI. Cells were analyzed by confocal microscopy (TCS SP5, Leica). The number of phagocytized beads per IBA-1-positive or P2RY12-positive cell was counted using image J software for phagocytic activity [34]. To assess phagocytosis cup formation in iMGs, cells were fixed by adding latex beads for 2 h. For live cell imaging of phagocytosis, iMG cells were grown in imaging dishes (Chamber Slide Lab-Tek II 4; Fisher) and labeled with 100 nM SiR-actin dye (for cytoskeleton staining; Cytoskeleton Inc., North America, USA) according to the manufacturer's protocol [35]. After washing twice with PBS, the old medium was replaced with fresh medium. Three microliters of latex beads (1.1 μm, Sigma-Aldrich) were added to the cells before analysis. Images were captured at a rate of one frame every 1 min 30 sec over a 5 h period. Live imaging was performed using a DeltaVision fluorescence microscopy system (Applied Precision) installed at the Hanyang Center for Research Facilities.

Isolation of human brain microglia from the neural tissue of sALS patients

We confirmed the microglia signature of iMGs that originated from monocytes from an sALS patient whose blood sample was collected just one day before death. We immediately isolated microglia from fresh brain tissue (brain-MG) from the same patient. The patient had no known pathogenic mutations, including *FUS*, *C9orf72*, *SOD1*, *ALS2*, *SPG11*, *UBQLN2*, *DAO*, *GRN*, *SQSTM1*, *SETX*, *MAPT*, *TARDBP*, or *TAF15* gene mutations. For brain-MG culture, the immediately-obtained fresh middle temporal gyrus was washed in HBSS. The tissue was then diced into ~1 mm^3 pieces using a sterile scalpel and transferred to a 50 ml falcon tube containing 10 ml enzyme dissociation mixture with 10 U/ml DNase (Invitrogen) and 2.5 U/ml papain (Worthington, NJ, USA) in Hibernate-A medium (Gibco) (per gram of tissue). The mixture was incubated at 37°C for 10 min with gentle rotation. The tissue was removed from the incubator, gently triturated to aid digestion, and returned to the incubator for a further 10 min. Dissociation was slowed by adding equal volumes of Dulbecco's modified Eagle medium and F-12 medium (DMEM/F12; Gibco) with 1% B27 (Gibco). The cell suspension was passed through a 70 μm cell strainer (Bector Dickinson, NJ, USA). Cells were centrifuged at 160 × *g* for 10 min. The supernatant was discarded and the cell pellet was resuspended in 20 ml DMEM/F12 with 1% B27, 1% GlutaMAX (Gibco), and 1% penicillin-streptomycin-glutamine (PSG; Gibco). Next, one-third volume of cold Ficoll (GE Healthcare, Little Chalfont, UK) was added to the cell suspension, and the tube was centrifuged at 4000 rpm for 30 min at 4°C. The interphase containing the microglia was transferred to a new tube (the myelin and erythrocyte layers were discarded) and washed twice with DMEM supplemented with 10% FCS, 1% Pen/Strep, 1% gentamycin, and 25 mM HEPES (Invitrogen). Negative selection of granulocytes (previous method only) and positive selection of microglia with anti-CD15- and anti-CD11b-conjugated magnetic microbeads (Miltenyi Biotec), respectively, were performed by magnetic activated cell sorting (MACS) according to the manufacturer's protocol [36]. Briefly, cells were incubated with 10 μl CD15 microbeads for 15 min at 4°C, washed, suspended in bead buffer (0.5% BSA, 2 mM EDTA in PBS, pH 7.2), and transferred to an MS column placed in a magnetic holder. The flow-through containing unlabeled cells was collected, washed, and incubated with 20 μl CD11b microbeads for 15 min at 4°C. The cells were then washed and placed on a new MS column in a magnetic holder. The $CD11b^+$ cell fraction was eluted by removing the column from the magnet, adding bead buffer, and emptying the column with a plunger. Acutely isolated primary microglia were suspended in Trizol reagent (Invitrogen) and stored at -80°C.

We isolated monocytes from the blood of the same patient using anti-CD14-conjugated magnetic microbeads (Miltenyi Biotec) according to the manufacturer's protocol. The isolated monocytes were suspended in Trizol reagent (Invitrogen) and stored at -80°C for RNA-seq and qPCR.

RNA sequencing and data analysis

Total RNA was isolated using Trizol reagent (Invitrogen). RNA quality was assessed with an Agilent 2100 bioanalyzer using an RNA 6000 Nano Chip (Agilent Technologies, Amstelveen, Netherlands). Control and

test RNA libraries were constructed using a SENSE 3' mRNA-Seq Library Prep Kit (Lexogen, Inc., Austria) according to the manufacturer's instructions. The library was amplified to add complete adapter sequences required for cluster generation. The constructed library was purified from PCR components. High-throughput sequencing was performed as single-end 75 sequencing using a NextSeq 500 platform (Illumina, Inc., USA). SENSE 3' mRNA-Seq reads were aligned using Bowtie2 version 2.1.0 [37]. Bowtie2 indices were generated either from genome assembly sequences or from representative transcript sequences aligned with the genome and transcriptome. The alignment file was used to perform transcript assembly, estimate gene abundance, and detect differential gene expression. Differentially expressed genes (DEGs) were determined based on counts from unique and multiple alignments using EdgeR in R version 3.2.2 and BIOCONDUCTOR version 3.0 [38]. Read count (RT) data were processed based on the global normalization method using Genowiz™ version 4.0.5.6 (Ocimum Biosolutions, India). Gene classification was based on searches performed in the DAVID (http://david.abcc.ncifcrf.gov/) and Medline (http://www.ncbi.nlm.nih.gov/) databases. We used MeV 4.9.0 to perform sample and gene clustering and to visualize gene clusters and heat maps. Hierarchical cluster analyses were performed using Euclidean distance as a similarity measurement with average linkage heuristic.

Cell culture

Human microglial clone 3 cells (HMC3 cells) (ATCC®CRL-3304) were cultured in Eagle's Minimum Essential Medium containing 10% FBS (Gibco) and antibiotics. HeLa cells were cultured in Dulbecco's modified Eagle's medium containing 10% FBS (Gibco), sodium bicarbonate, sodium pyruvate (Sigma), and antibiotics. HeLa cells were transiently transfected with GFP-tagged human NCKAP1 cDNA constructs or with NCKAP1 shRNA using Lipofectamine® 2000 (Invitrogen) according to the manufacturer's protocol. For human NCKAP1 overexpression or knockdown experiments, cells were transduced with pLenti-C-mGFP-Human NCK-associated protein 1 (NCKAP1, NM_013436), cDNA ORF Clone (OriGene Technologies, Rockville, MD, USA), or pGFP-C-shLenti-NCKAP1 Human shRNA lentiviral particles (Gene ID 10787, OriGene Technologies) two days before analysis according to the manufacturer's protocol.

Immunoblotting

Cells were washed twice with PBS and incubated on ice in RIPA buffer for 10 min. Equal amounts of protein from each sample were separated by SDS-PAGE and transferred to a PVDF membrane (GE Healthcare). The membrane was blocked with 5% skim milk and incubated with the following primary antibodies: rabbit anti-NCKAP1 (Novus Biologicals, NBP1-83269, 1:1000), rabbit anti-CYFIP1 (Sigma, SAB2700152, 1:1000), mouse anti-WAVE2 (Santa Cruz, sc-373889, 1:200), rabbit anti-WAVE1 (Sigma, SAB4503508, 1:1000), mouse anti-ABI (Santa Cruz, sc-398554, 1:1000), and anti-GAPDH (Santa Cruz, SC-25778, 1:1000). Membranes were washed with Tris-buffered saline containing 0.05% Tween-20 and

processed using a horseradish peroxidase (HRP)-conjugated secondary anti-rabbit or -mouse antibody (Amersham Pharmacia Biotech) followed by enhanced chemiluminescence (ECL) detection (Amersham Pharmacia Biotech). Western blot results were quantified with an image analyzer (Quantity One-4, 2, 0; Bio-Rad) and normalized to GAPDH expression. The reported results are based on three independent experiments done using separate batches of cells.

Enzyme-linked immunosorbent assay

Secretion of pro- and anti-inflammatory cytokines (TNF-α, IL-1β, IL-6, IL-10, and TGF-β1) during LPS stimulation from culture supernatants was tested using a commercially available cytokine assay kit obtained from Millipore (Billerica, MA), according to the manufacturer's protocol. Human IL-6, interferon (IFN)-γ, IL-8, TNF-α, and CCL2/MCP-1 (R&D Systems) were used to determine cytokine concentration in plasma samples of patients with ALS and healthy controls according to the manufacturer's instructions. Each assay was performed in triplicate.

miRNA mimics and inhibitor transfection

miR-214 and miR-34 mimics or inhibitors and control oligonucleotides were synthesized by Bioneer Corporation (Daejeon, Korea). Their sequences are as follows: miR-214-3p mimic, 5'-UGCCUGUCUACACUUGCUGUGC-3'; miR-34c-3p mimic, 5'-AAUCACUAACCACACGGC AGG-3'; miRNA mimic negative control #1 (SMC-2003); miR-214-5p inhibitor, 5'-UGCCUGUCUACACUUGCUGUGC-3'; miR-214-3p inhibitor, 5'-ACAGCAGGCACAGA CAGGCAGU-3'; miR-34c-3p inhibitor, 5'-AAUCACUAACCACACGGCCAGG-3'; and miRNA inhibitor negative control #1 (SMC-2103). Synthetic miRNA mimics, inhibitors, and the negative control were transfected into HeLa cells using Lipofectamine® RNAiMAX (Invitrogen) according to the manufacturer's instructions. Briefly, 50 nM miRNA mimic, miRNA inhibitor, or negative control were transfected into cells plated at 3×10^5 cells/well in 6-well plates.

Plasma miRNA analysis

The small RNA-enriched fraction was extracted from 625 μl of the plasma sample using a mirVana miRNA isolation kit, following the manufacturer's instructions (Ambion, Austin, TX). The purity of the extracted RNA was quantified using a NanoDrop™ 1000 spectrophotometer. For reverse transcription and quantitative real-time PCR, a fixed volume of 5 μl of the small RNA-enriched fraction obtained from a given sample was used for the reverse transcription (RT) reaction. For synthesis of each miRNA-specific cDNA, miRNA was reverse transcribed using the TaqMan miRNA reverse transcription kit (Life Technologies). The following primers were used for endogenous controls (Life Technologies): hsa-miR-214-3p (4427975, ID002306) and hsa-miR-34c-3p (4427975, ID 241009_mat). The reaction mixture was

incubated at 16°C for 30 min, 42°C for 30 min, and 85°C for 5 min. TaqMan™ (Life Technologies) assays were used to quantify mature miRNA transcripts according to the manufacturer's recommendations. PCR experiments were performed using an Applied Biosystems Step One Plus^{TM} system (Life Technologies) under the following cycling conditions: 95°C for 10 min with 45 cycles of 95°C for 15 s and 60°C for 1 min. Data analysis was performed to determine the threshold cycle (Ct). Relative quantities of miRNA were calculated using the $2^{-\Delta\Delta Ct}$ method after normalization to hsa-miR-16 levels in plasma samples.

Statistical analysis

Data are presented as mean ± SEM. The statistical significance of differences between groups was assessed with Student's *t*-test, one way-ANOVA, and two way-ANOVA using GraphPad Prism 7 (GraphPad Software, San Diego, CA). The findings were regarded as significant when *$p < 0.05$, **$p < 0.01$, ***$p < 0.001$, and **** $p < 0.0001$. In *post-hoc* analysis, *p*-values were obtained by Pearson correlation.

Results

Healthy control (HC)-iMGs present the main signatures of microglia and show intrinsic functions

As shown in the schematic diagram of our successive experiments (Additional file 2: Figure S1), we generated human iMGs from PBMCs obtained from five healthy controls (HCs) treated with inducible supplements consisting of IL-34 and GM-CSF; the PBMCs were cultured for 3 weeks to induce a more mature form of microglia-like cells. The generated iMGs displayed well-ramified morphology after 21 days in culture (Fig. 1a, Additional file 4: Figure S2). They were conventionally identified as $CD11b^{+}$ $CD45^{low}$ cells by flow cytometry analysis (Fig. 1b). They were characterized by upregulated expression of resident microglia surface markers including P2RY12 and IBA-1 in immunofluorescence analysis. The monocyte marker CCR2 disappeared from iMGs (Fig. 1c). In qRT-PCR findings, key signatures of microglia, such as *P2RY12, OLFML3, TGFBR1,* and *TREM2,* were significantly upregulated in iMGs compared to monocytes (Fig. 1d). mRNA levels of inflammation-related factors were altered in iMGs upon induction with IL-4, LPS, or dexamethasone, which is consistent with observations from a previous post-mortem microglial study (Fig. 1e) [32]. In addition, iMGs showed normal phagocytic function and increased expression of *TNF-α* mRNA upon stimulation with latex beads (Fig. 1f and g). The optimal culturing time period and minimal blood sample amounts to be used in serial subsequent studies for the preparation of iMGs from ALS patients were identified based on trial and error data achieved from the HC-iMGs model.

Although our data and the results of previous studies [23, 26] suggest that HC-iMGs present key signatures of microglia and show intrinsic microglial functions, it is unclear whether iMGs derived from PBMCs accurately reflect brain microglia in the same person. To address this key question, blood was obtained from a patient with sALS just before death who consented to his body being donated. Brain

microglia from that patient were immediately isolated from autopsy tissue using CD11b beads. These samples were used in the next experiment.

-

iMGs express key genetic signature of brain microglia

To identify similarities between iMGs and brain microglia, we obtained fresh brain tissue and peripheral blood from a patient with sALS, and then performed RNA sequencing (RNA-seq) of iMGs, brain microglia (brain-MG, $CD11b^{+}$), and monocytes ($CD14^{+}$) (Fig. 2a). Whole-transcriptome differential gene expression analysis revealed 13,038 genes that had a greater than 3-fold difference in either iMGs or brain-MG compared to monocytes. Of these, 705 (5.4%) overlapped between iMGs and brain-MG (Fig. 2b, Additional file 5: Table S3). In comparison, only 195 (1.5%) of the enriched genes overlapped between iMGs and monocytes. Hierarchical clustering analysis revealed similarities between iMGs and brain-MG (Fig. 2c). Through gene ontology (GO) analysis of the 705 overlapping genes, we found ten significant pathway modules that were commonly expressed in both iMGs and brain-MG. These represent gene subsets related to extracellular matrix organization, metabolic processes, oxidation-reduction processes, cell migration, and inflammatory responses (Fig. 2d, Additional file 5: Table S4). Searching the Kyoto Encyclopedia of Genes and Genomes (KEGG) database revealed ECM-receptor interactions, metabolic pathways, and focal adhesion (Fig. 2d, Additional file 5: Table S4). Regarding microglial signature genes [39], the expression levels of *SPP1, JUN, TREM2, APOE, HEXB, MEF2A, LILRB4, CX3CR1, ITGAX, TGFBR1, P2RY12, MAFB, TGFB1,* and *SLCO2B1* in iMGs were similar to those in brain-MG, although the expression levels of *OLFML3, AXL, CSF1R, RHOB, EGR1,* and *TMEM119* in iMGs were relatively low (Fig. 2e). Immunofluorescence staining showed that P2RY12, IBA-1, and the transcription factor PU.1 were well preserved in both iMGs and brain-MG, although immunoreactivity (IR) of TMEM119 in iMGs was less than in brain-MG (Fig. 2f).

ALS(R)-iMGs show dystrophic morphology and severely impaired phagocytic function

To verify our hypothesis that microglial dysfunction was associated with the speed of progression of ALS, we generated iMGs from three HCs (C1 – C3) and eleven patients with sALS [6 slowly progressing ALS(S) (S1 – S6) and 5 rapidly progressing ALS(R) (R1 – R5) patients]. Their demographic characteristics are summarized in Additional file 1: Table S1. The participants enrolled in this first step study were assigned into “group #1” (Additional file 2: Figure S1). To exclude the possibility of genetic effects on ALS progression, sALS patients were only enrolled after confirming that they had no familial history of ALS or ALS-related major known genetic mutations based on whole exome sequencing (WES). The genetic panel included *SOD1*, *ALS2*, *TDP-43*, *FUS, C9orf72,* and *OPTN* (Additional file 3: Table S2).

The expression of genes related to homeostatic microglial function (*P2RY12, OLFML3, TGFBR1, GPR34, MERTK, HEXB,* and *CSF1R, and TMEM119*) was not significantly different between ALS(S)-iMGs and

ALS(R)-iMGs, although the expression levels of several genes were decreased compared to those in HC-iMGs (Fig. 3a). Immunocytochemical staining showed that P2RY12, a representative microglia-specific gene signature [40], was well preserved in both iMGs from both ALS groups (Fig. 3b). Despite the lack of expression level differences in microglial signature genes between iMGs from the two ALS groups, Imaris-based morphometric analysis revealed that ALS(R)-iMGs were significantly different from ALS(S)-iMGs and HC-iMGs (Fig. 3c). Based on morphological parameters for dynamic microenvironment surveillance, dendritic length, number of segmentations, branching, and dendritic terminal points were significantly reduced in both ALS group-iMGs compared to HC-iMGs. However, the number of branches and terminal points were markedly reduced in ALS(R)-iMGs compared to ALS(S)-iMGs, although there was no difference in cell area of iMGs between the two ALS groups and HC. Furthermore, phagocytic function was compared between ALS(S)-iMGs and ALS(R)-iMGs. The most remarkable finding was that phagocytic function was severely impaired in ALS(R)-iMGs, whereas ALS(S)-iMGs exhibited no significant differences in phagocytic function compared to HC-iMGs (Fig. 3d, e, and Additional file 6: Figure S3).

Next, to exclude the possibility of senescence-related factors leading to phagocytic dysfunction of microglia [41], we compared the expression levels of senescence-related genes using qRT-PCR. There was no difference between ALS(S)-iMGs and ALS(R)-iMGs in the expression of the cellular senescence markers $p21^{CIP1}$ *and* $p16^{INK4}$, and there was no difference in age at sampling time between the patient groups (Fig. 3f, Additional file 2: Table S1). Thus, we ruled out aging as a factor in the defective phagocytic function shown in ALS(R)-iMGs

Defective phagocytosis in ALS(R)-iMGs is associated with decreased NCKAP1 expression

Next, we performed comparative transcriptome analysis to identify molecular targets involved in phagocytic dysfunction of ALS(R)-iMGs after generating a second set of iMGs (group #2, Additional file 2: Figure S1) from four patients with ALS(S) (S7 – S10), three patients with ALS(R) (R6 – R8), and three HCs (C1 – C3). The second set of ALS(R)-iMGs also showed phagocytic dysfunction (Additional file 6: Figure S3).

Whole-transcriptome differential gene expression analysis revealed 4,367 genes with a 1.5-fold difference in expression in this analysis (Fig. 4a). The proportion that overlapped between ALS(R)-iMGs and ALS(S)-iMGs was 19.7% (861 genes). GO analysis of those 861 genes revealed that they were related to immune response, regulation of NF-κB transcription factor activity, innate immune response, etc. (Additional file 5: Table S5). Importantly, we found that 2,559 transcripts were significantly different between ALS(R)-iMGs and ALS(S)-iMGs (Additional file 5: Table S6). GO analysis of the 2,559 genes revealed gene subsets including those involved in chemotaxis, cilium assembly, long-chain fatty-acyl-CoA biosynthesis, response to lipopolysaccharide, inflammatory responses, actin filament polymerization, immune responses, metabolic processes, the Fc-gamma receptor signaling pathway involved in phagocytosis, and phagocytosis. KEGG pathways included metabolic pathways, focal adhesion, ECM-receptor interactions,

ubiquitin-mediated proteolysis, and cytokine-cytokine receptor interactions (Fig. 4b, Additional file 5: Table S7).

Thus, we speculated that subsets of genes involved in chemotaxis, actin filament polymerization, phagocytosis, focal adhesion, ECM receptor interactions, and immune-related pathways might be associated with defective phagocytosis in ALS(R)-iMGs. When we used GO to focus on phagocytosis-related pathways and genes, heatmap analysis revealed that genes including *NCKAP1*, *VAV3*, *MYO10*, *FYN*, *ARPCA1*, and *SLC11A1* were significantly down-regulated in ALS(R)-iMGs compared to ALS(S)-iMGs (Fig. 4c). Moreover, *MFGE8*, *PTX3, GAS6*, *FCGR2B*, and *CD36* were upregulated in ALS(R)-iMGs. To confirm these results, we analyzed mRNA expression levels of these major genes using all available samples from both group #1 and #2 (Fig. 4d). Interestingly, NCK-associated protein 1 (*NCKAP1*) and Guanine Nucleotide Exchange Factor Vav 3 (*VAV3*), known intracellular signaling-regulated factors related to the actin-polymerization process after the initial recognition step in phagocytosis [42], were significantly decreased in ALS(R)-iMGs. Moreover, ALS(R)-iMGs had decreased *TREM2* levels, which may partially contribute to defects in phagocytic function. However, levels of *MFGE8* and *PTX3*, recognition and enhancing factors in phagocytosis, were elevated.

As shown in Fig. 4c-e, the transcript showing the greatest difference in ALS(R)-iMGs was NCKAP1, which is a key component of the actin polymerization process related to the phagocytic machinery. The low level of *NCKAP1* mRNA noted in ALS(R)-iMGs does not reflect an intrinsic characteristic of monocytes, which rarely express NCKAP1 [43]. This finding was supported by the data showing high expression of *NCKAP1* mRNA in ALS(S)-iMGs (Fig. 4e). Additionally, *NCKAP1* was highly expressed in HMC3 cells and iMGs compared to monocytes (Additional file 7: Figure S4). This result suggests that NCKAP1 is the most important factor related to defective phagocytosis. Thus, we further investigated the critical role of the *NCKAP1* gene in phagocytosis. In the next step, we generated another new set (“group #3”) of iMGs from four patients with ALS(S) (S11 – S14) and seven patients with ALS(R) (R9 – R15) (Additional file 2: Figure S1).

NCKAP1 regulates actin polymerization during the phagocytic process in iMGs

To further delineate the role of NCKAP1 in phagocytosis, ALS(R)-iMGs (R9 – R15) and ALS(S)-iMGs (S11 – S14) were transfected with GFP vector, shNCKAP1-GFP, or NCKAP1-GFP and subsequently cultured for 72 hours. The efficiency of NCKAP1 knockdown in HeLa cells and iMGs was evaluated by qRT-PCR (Additional file 8: Figure S5a and b). Knockdown was also confirmed by immunofluorescence analysis (Additional file 8: Figure S5c). NCKAP1-GFP-transfected cells showed intense IR of phalloidin, a filamentous actin (F-actin) marker, which was absent from shNCKAP1-transfected cells. These findings suggest that NCKAP1 is involved in the formation of F-actin. Similar findings were reproduced in both ALS(S)- and ALS(R)-iMGs (Additional file 8: Figure S5d). Decreased levels of NCKAP1 and phalloidin IR were noted in ALS(R)-iMGs compared to ALS(S)-iMGs (upper figures). However, transduction of

shNCKAP1 reduced IR of both phalloidin and NCKAP1 in ALS(S)-iMGs, and the opposite was true in NCKAP1-GFP-transfected ALS(R)-iMGs (lower figures).

NCKAP1 is a known member of the WAVE regulatory complex (WRC) [44]. Thus, we investigated the relationship between NCKAP1 and other actin polymerization-related genes and the effect of NCKAP1 overexpression or knockdown on the expression of related molecules such as cytoplasmic FMR1-interacting protein 1 (CYFIP1), Abelson interactor 2 (ABI2), WASP-family verprolin homologous protein 1 (WAVE1), and WAVE2 using iMGs from "group #3." As shown in Fig. 5a and b, NCKAP1 accumulated at the F-actin-rich apical region of the cell membrane (represented as phalloidin, WAVE) which formed a phagocytic cup during phagocytosis in ALS(S)-iMGs (white dot-lined box and white arrow). Phagocytic cup formation is involved in actin polymerization under the plasma membrane in the initial engulfment step of phagocytosis. This was clearly observed in ALS(S)-iMGs incubated with latex beads. In addition, F-actin-rich cup-like structures co-localized with NCKAP1 (upper figures of Fig. 5a). In contrast, ALS(R)-iMGs exhibited considerably fewer phagocytic cups with accumulated F-actin at the regions of contact with latex beads (bottom of Fig. 5a). Immunofluorescence revealed that WAVE complexes, such as WAVE and ABI, co-localized with NCKAP1 in ALS(S)-iMGs but not in ALS(R)-iMGs (Fig. 5a and b). Next, to evaluate the role of NCKAP1 in WAVE complex stability, we transfected HeLa cells with GFP-tagged NCKAP1 or GFP-tagged NCKAP1 shRNA and then performed Western blots to determine the effects of NCKAP1 on actin polymerization-related proteins. We found that NCKAP1 overexpression increased expression of actin polymerization-related proteins (CYFIP1, ABI2, WAVE1, and WAVE2), whereas NCKAP1 knockdown reduced their expression (Fig. 5c and d).

Finally, we examined whether NCKAP1 overexpression rescued the defective phagocytic function of ALS(R)-iMGs using live cell imaging. While phagocytosis of latex beads was clearly present in ALS(S)-iMGs (upper part of Fig. 5e), ALS(R)-iMGs showed defective phagocytosis (bottom part of Fig. 5e). On the contrary, when NCKAP1 was overexpressed using NCKAP1-GFP in ALS(R)-iMGs, phagocytosis was rescued. As expected, the active phagocytosis seen in ALS(S)-iMGs was not present when NCKAP1 was knocked down with shNCKAP1-GFP. These findings are evident in snapshot images (Fig. 5e and f) and live cell images (Additional file 9-12: Video S1-4). Collectively, our data suggest that NCKAP1 plays a pivotal role in the formation of phagocytic cups by participating in the WAVE complex-mediated actin polymerization process. Thus, NCKAP1 is an important potential biomarker that could be useful for predicting the state of perturbed phagocytic function of iMGs in rapidly progressing ALS patients.

ALS(R)-iMGs have an exaggerated response to inflammatory signaling

Phagocytosis is traditionally regarded as beneficial for tissue homeostasis; it is responsible for rapid clearance of dying cells or debris, thus preventing spillover of pro-inflammatory and neurotoxic responses [42]. Transcriptome analysis showed that the immune response pathway, which operates in response to LPS and inflammatory signaling, functions differently in iMGs from the two ALS groups, as shown in Fig. 4b. Thus, we compared the mRNA expression levels of cytokines in response to LPS stimulation in

ALS(S)-iMGs and ALS(R)-iMGs in “group #1” samples after confirming that our culture environment could mirror the differential phenotypes [Additional file 13: Figure S6]. In the unstimulated state, there was a significant difference in mRNA levels of the cytokines (*TNF-α*, *IL-6*, *TGF-β1,* and *IL-10*) between both ALS groups and monocytes, and the difference was reproduced in iMGs [Additional file 14: Figure S7]. In addition, LPS stimulation provoked an increase in mRNA expression of pro-inflammatory cytokines and a decrease in *TGF-β* expression in iMGs from both ALS groups. ALS(R)-iMGs exhibited an exaggerated *TNF-α*, *IL-6*, *IL-1β*, and *TGF-β* response compared to ALS(S)-iMGs upon LPS stimulation (Fig. 6a). Cytokine levels in the culture media showed a pattern that was similar to the mRNA expression profiles, as measured by ELISA (Fig. 6b). These findings suggest that the response of ALS(R)-iMGs to an inflammatory stimulus is exaggerated in comparison to the response of ALS(S)-iMGs.

To address whether the enhanced pro-inflammatory response seen in ALS(R)-iMGs is associated with decreased NCKAP1 expression, we examined the causal relationship between key inflammatory signals and NCKAP1. Because we had no frame of reference regarding the role of NCKAP1 in microglial function and inflammatory signaling, we speculated that NCKAP1 might show similar acting with NCKAP1L (NCKAP1-like). NCKAP1L and NCKAP1 belong to the same family and have similar structures. NCKAP1L is known as a crucial player in actin polymerization. It is selectively expressed in hematopoietic cells [45]. Recently, NCKAP1L was proposed to be a novel phagocytosis regulator in a phagocyte cell line [46]. Furthermore, NCKAP1L is a common upstream signal with NF-κB, which is a representative inflammatory signal in hematopoietic cells [47]. Thus, we studied whether NCKAP1 reduction is involved in NF-κB signaling in ALS(R)-iMGs. We examined NF-κB signaling in response to LPS stimulation in ALS(R)-iMGs. *NF-κB p-50* and *p-65* mRNA expression levels were strongly upregulated in ALS(R)-iMGs upon LPS stimulation (Fig. 6c). Overall, our results indicate that NCKAP1 reduction may be related to the abnormally exaggerated inflammatory response via the NF-κB signaling pathway. This finding provides a clue as to why an enhanced pro-inflammatory response is present in ALS(R)-iMGs.

In sum, we concluded that NCKAP1 reduction induced defective phagocytic function and exaggerated the pro-inflammatory response in ALS(R)-iMGs. In addition, NCKAP1 levels in iMGs could reflect the state of clinical progression of ALS. However, measurement of NCKAP1 activity is possible only after a time-consuming process of generating iMGs. Thus, it cannot be used as a marker for the speed of progression of ALS in a practical context. To find more useful possible biomarkers related to NCKAP1 activity that can predict the speed of clinical progression of ALS, serial subsequent studies were undertaken. After rechecking that no *NCKAP1* mutations or pathogenic polymorphisms were detected in the WES results of 29 ALS patients (Additional file 1: Table S1), we searched for serologically available biomarkers related to NCKAP1 expression.

miRNA-214-3p and miRNA-34-3p targeting NCKAP1 are associated with NCKAP1 reduction

After excluding the possibility of *NCKAP1* mutations, we searched for miRNA candidates that regulate NCKAP1 expression. miRNA targets were predicted by combinatorial utilization of two different web-

based prediction algorithms, TargetScan and miRanda. We also collected targets that had been experimentally confirmed *in vitro* along with ALS-related and inflammation-related miRNAs from published studies. miR-214-3p and -34c-3p were selected as candidates. The two micro-RNAs can directly reduce NCKAP1 expression [48, 49]. Herein, we identified a putative miR-214-3p and -34c-3p binding site in the 3'-UTR of NCKAP1 using bioinformatics tools for miRNA target prediction (Fig. 7a). To determine whether miR-214-3p and -34c-3p directly target NCKAP1, the effects of miR-214-3p and -34c-3p mimics and inhibitors were tested in HeLa cells for their effects on *NCKAP1* gene expression. As shown in Fig. 7b, both miR-214-3p and -34c-3p downregulated NCKAP1, while the inhibitors upregulated NCKAP1. Both miRNAs were strongly expressed in iMGs (Additional file 7: Figure S4). This finding indicates that both miR-214-3p and miR-34c-3p play a role in regulating NCKAP1 levels.

Based on the serial experimental results, we selected NCKAP1 and its regulators (miR-214-3p and -34c-3p) as candidate biomarkers that reflect the phagocytic function of ALS-iMGs and the clinical progression of ALS. To validate our findings, *post-hoc* comparative analysis was done to address whether clinical data on the enrolled participants (groups #1, 2, 3) correlated with the selected miR candidates. As shown in Fig. 7c, plasma levels of miR-214-3p and -34c-3p were increased in both ALS groups compared to HCs. Additionally, both miRNAs were significantly increased in ALS(R) compared to ALS(S) (plasma miR-214-3p: $p = 0.043$; plasma miR-34c-3p: $p = 0.021$).

Finally, we analyzed the relationship between each patient's speed of clinical progression, expressed as delta-FS (points/month), and the activity of the three biomarkers (*NCKAP1*, miR-214-3p, and miR-34c-3p). All three markers were well correlated with each patient's delta-FS (plasma miR-214-3p: $r = 0.444$, $p = 0.016$; plasma miR-34c-3p: $r = 0.518$, $p = 0.004$; *NCKAP1*: $r = -0.676$, $p = 0.011$; Fig. 7d). Thus, speed of disease progression was inversely correlated with *NCKAP1* expression, while miR-214-3p and miR-34c-3p were positively correlated with disease progression. When the relationship between *NCKAP1* and each miRNA was evaluated, only miR-214-3p was negatively correlated with *NCKAP1* ($r = -0.520$, $p = 0.034$, Fig. 7e). Taken together, these findings suggest that decreased *NCKAP1* expression in iMGs and a concomitant increase in plasma miRNA-214-3p levels are correlated with rapid progression in ALS patients.

In summary, our data indicate that the perturbed phagocytic function seen in ALS(R)-iMGs is related to decreased NCKAP1-mediated impairment of proper actin polymerization. Regarding serological biomarkers related to NCKAP1, *post-hoc* analysis indicated that delta-FS, representing the speed of progression of ALS, correlates well with each patient's biomarkers, including *NCKAP1*, plasma miRNAs, and inflammatory cytokines. Thus, targeting microglial *NCKAP1* may be an alternative therapeutic target in rapid sALS. In addition, miRNA-214-3p could be a serologic biomarker that is clinically useful for predicting the speed of progression of ALS. Our current hypothesis regarding the involvement of the microglial pathway in rapid progression of ALS is summarized graphically in Fig. 7f.

Discussion

The significance of the current study is that we identified serologically reliable biological markers and possible therapeutic targets associated with defective microglial functioning in rapidly progressing ALS using an induced microglia-like cell model. Using transcriptome analysis, we identified defective phagocytosis corresponding with reduced *NCKAP1* levels as the key factor that gave rise to phagocytic dysfunction in ALS(R)-iMGs. Though there was no significant difference in major homeostatic gene profiles between the two groups of ALS-iMGs, as shown in Fig. 3a, *NCKAP1* levels were reduced in both groups of ALS-iMGs as compared with HC-iMGs. Only ALS(R)-iMGs showed intrinsically perturbed phagocytosis and an exaggerated inflammatory response via increased NF-κB signaling in response to LPS stimulus. These data imply that *NCKAP1* reduction in ALS(R)-iMGs may be responsible for both defective phagocytosis and the accelerated inflammatory response in a pro-inflammatory environment, a well-known condition in ALS. This result is supported by data on ALS(S)-iMGs showing intact phagocytic function with less of a pro-inflammatory response than is present in ALS(R)-iMGs.

Given that activated inflammatory responses and excessive oxidative stress are commonly encountered environments in ALS, it is understandable that previously reported data suggests that the progression of ALS is correlated with the activity of pro-inflammatory cytokines [12, 50]. These findings agree with our *post-hoc* data, which revealed that rapidly progressing ALS patients with perturbed phagocytosis in their iMGs also showed an increase in plasma levels of the pro-inflammatory cytokine IL-8 compared to the slowly progressing ALS group, as shown in Additional file 15: Figure S8. Moreover, the rate of disease progression (delta FS) was also correlated with the level of plasma IL-8 (Additional file 15: Figure S8f).

We looked at the steps of the phagocytic process using transcriptome analysis and found that mRNA levels of *MFGE8,* a recognition receptor [51], and *PTX3,* an enhancer of microglial phagocytic activity [52], were significantly higher in ALS(R)-iMGs despite their defective phagocytic functioning. Another interesting finding was that expression of *TREM2*, a well-known risk gene related to microglial phagocytic function in Alzheimer's disease (AD) [53, 54], Parkinson's disease (PD) [55], and ALS [56], was decreased in ALS(R)-iMGs, as shown in Fig. 4d. These data also imply that compensatory mechanisms that are activated in response to perturbations in phagocytosis work by elevating the levels of recognition molecules (*MFGE8* mRNA) or by enhancing microglial phagocytic activity, such as that involving *PTX3* mRNA; concomitant decreases in *TREM2* activity and *NCKAP1*-mediated improper actin polymerization may contribute to the defective phagocytic function seen in ALS(R)-iMGs.

Only a few studies have reported an association between NCKAP1 and neurodegenerative diseases; for example, *NCKAP1* gene expression is known to be reduced in AD [57]. Most studies of NCKAP1 have focused on its role in neuronal differentiation and migration as a cytoskeletal regulator during development [58]. Furthermore, *NCKAP1L*, a hematopoietic cell-specific gene that has a similar structure to *NCKAP1*, has been reported as a key player in actin polymerization. It is also essential for neutrophil and macrophage migration and phagocytosis [43, 45, 46]. NCKAP1L family members are known to regulate actin polymerization, morphogenesis, and immunity [45]. Both NCKAP1 and NCKAP1L are members of the WRC that consists of Abi (Abelson interactor 1 or 2), WAVE (WAVE 1, 2, 3), Sra1

(specifically Rac-associated protein 1), and activated Arp2/3 (actin-related protein-2/3), all of which can promote actin polymerization. In contrast to NCKAP1L, NCKAP1 is enriched in the brain, but absent or less expressed in hematopoietic cells [47]. Our results showed that ALS(R)-iMGs overexpressing NCKAP1 exhibited restored phagocytic function and increased expression levels of CYFIP1, ABI2, WAVE1, and WAVE2. Because the stability of WRC is interdependent on the presence of individual WRC components [45], low NCKAP1 expression may cause instability of the complex and hinder F-actin polymerization in microglia-like cells. Therefore, NCKAP1 is presumed to play a key role in the engulfment process of phagocytosis by regulating actin cytoskeleton dynamics.

Numerous studies have focused on toxic microglia as a factor in ALS progression. Reactive microglia can aggravate motor neuron death through pro-inflammatory cytokine secretion in *SOD1* mice. Depletion of defective microglial cells can resolve neuroinflammation and result in prolonged survival [59]. Additionally, ALS(R)-iMGs showed an intense pro-inflammatory reaction to LPS stimuli, in accordance with the results of previous *SOD1* mouse and human studies [10, 60, 61]. This reaction is distinct from the general characteristics of aged microglia [39, 62]. The exaggerated pro-inflammatory response of ALS(R)-iMGs to LPS stimuli (like immune vigilance) [41] may be associated with reduced expression of *NCKAP1* and related WRC genes. In the hematopoietic system, cytokine expression via NF-κB signaling and actin polymerization for phagocytosis have a common upstream signaling molecule, Rac small GTPase. However, these two pathways bifurcate upstream of Rac [45]. Thus, Rac activation by LPS can induce both NF-κB signaling and phagocytosis. However, reduced expression of NCKAP1 and the resulting decrease in actin polymerization-related proteins may shift Rac-GTP signaling toward NF-κB signaling, causing NF-κB over-activation and increased levels of pro-inflammatory cytokines in microglia. Our results support this speculation. ALS(R)-iMGs exhibited lower *NCKAP1* expression but higher NF-κB expression upon LPS stimulation than did ALS(S)-iMGs. Similar findings were observed in neurodegeneration-associated molecular patterns (NAMPs) [63], including mutant *SOD1*, *FUS*, *TDP-43*, RNA foci and RAN dipeptides, and degenerating neuronal debris. NAMPs may trigger a chronic inflammatory milieu in CNS, while microglia acting under acute inflammatory conditions in response to LPS have distinct activation profiles [64].

We searched for biological markers that could predict the speed of progression of ALS, and selected miRNA-214-3p and miRNA-34c-3p as reliable candidates. Both can directly reduce the level of *NCKAP1* expression [48, 49], in agreement with our results. Specifically, miRNA-214-3p expression was increased in microglia isolated from *SOD1*-G93A mice [65] and in muscles [66] and sera [67] of ALS patients. This miRNA acts as an inflammatory mediator that induces NF-κB activation and IL-6 expression [68]. miRNA-34c-3p also represses the expression of sirtuins (SIRTs). SIRT1 inhibits NF-κB activation upon inflammation in neurodegenerative disease states [69]. Our results suggest that the increased expression of miRNA-34c-3p and miRNA-214-3p that is seen in the plasma of patients was associated with rapidly progressing ALS, resulting in possibly targeting microglial *NCKAP1*. Thus, *NCKAP1* and miRNA-214-3p could be alternative therapeutic targets and reliable biological markers that reflect the speed of progression of ALS.

Our study leaves several unanswered questions. Although we propose the utility of the serological biomarkers miRNA-214-3p and miRNA-34c-3p, which inhibit NCKAP1 expression in an inflammatory environment, we did not clarify how *NCKAP1* was reduced in only ALS(R)-iMGs in our culture environment. One possible mechanism is through maintenance of epigenetic memory during direct conversion [70]. Direct conversion methods, including ours, have an advantage in that they preserve the aging-associated features of the donors, while iPSC models alter the epigenetic landscape during rejuvenation [71]. Further studies are needed to clarify whether our model maintains epigenetic memory. The next question is whether our culture media reflect CNS microenvironment of ALS patients. To address this issue, we confirmed that our culture environment could form pro-inflammatory environment and which was associated with GM-CSF (10 ng/mL) and IL-34 (100 ng/mL) for iMG generation. In fact, GM-CSF-treated monocytes express an inflammatory phenotype that includes secretion of pro-inflammatory cytokines, in agreement with previous studies [72, 73]. Thus, *NCKAP1* reduction by miRNA-214 and miRNA-34 in ALS(R)-iMGs is another possible mechanism for the observed defective phagocytic function, although we did not examine miRNA levels in ALS(R)-iMGs owing to the limited quantity of available samples. Another limitation of this study is related to the isolation of brain microglia from ALS patients using CD11b-positive beads that was done in order to compare the brain microglia with our iMGs model. These cells might be a mixture of infiltrated macrophages and resident microglia. In addition, we cannot exclude the possibility that the inflammatory characteristics of monocytes in rapidly progressing ALS patients [50] might contribute to the characteristics of our iMGs, despite the fact that *NCKAP1* expression in the monocytes of ALS patients is rare. There is still an argument that the iMGs model is closer to infiltrated blood-derived macrophages than resident microglia [23]. A third limitation is that iMGs are not absolutely identical to resident brain microglia. They cannot precisely reflect the characteristics of yolk sac-originated resident microglia in the non-diseased brain [74]. To overcome these inevitable hurdles of iMGs, studies focusing on the development of new, detailed markers that can discriminate iMGs from or correlate iMGs with microglia subpopulations [9] and diverse macrophage populations are needed. More precise single cell assay-based analytic approaches to the study of iMGs are needed.

Despite these limitations, our results revealed many similarities of iMGs with microglia, including intrinsic phagocytic functions and major signature gene profiles, that were demonstrated in our *in vitro* model and autopsied brain sample from an ALS patient. In addition, our iMGs model has an advantage in that it can be used to predict current complex inflammatory conditions associated with resident microglial phagocytic functions which iMGs share with infiltrating macrophages/monocytes. The interaction of infiltrated leukocytes with resident microglia could be considered a current outcome or status of neuroinflammation *per se* for predicting the pathophysiological process and speed of disease progression in ALS patients [13]. Therefore, our iMGs model may be a useful tool for indirectly understanding some aspects of microglial phagocytic function in ALS patients who exhibit different phenotypes. Moreover, this model can provide new insights into the multifaceted nature of microglia and microglial phagocytosis in ALS.

Conclusions

We speculate that the enhanced inflammatory milieu in rapidly progressing ALS patients increases miRNA-214-3p and miRNA-34c-3p levels, leading to reduced expression of *NCKAP1* in microglia. This may interfere with the engulfment step of phagocytosis and induce immune vigilance in rapidly progressing ALS. In addition, an increase in plasma levels of miRNA-214-3p was closely correlated with the clinical speed of progression in ALS patients and with *NCKAP1* expression in their iMGs. Therefore, *NCKAP1*-mediated disruptions in phagocytosis may be a good therapeutic target in ALS. Furthermore, our data indicate that miRNA-214-3p is an easily measurable biomarker that reflects the speed of progression of ALS.

List Of Abbreviations

ALS(S): slowly progressing ALS; ALS(R): rapidly progressing ALS; iMG: Microglia-like cell induced by monocyte; NCKAP1: NCK-associated protein 1; NCKAP1L: NCK-associated protein 1 like; DEGs: Differentially expressed genes; WES: whole exome sequencing; WAVE: WASP-family verprolin homologous protein; WRC: WAVE regulatory complex

Declarations

Ethics approval and consent to participate

This study was conducted in accordance with the World Medical Association's Declaration of Helsinki. It was approved by the Ethics Committee of Hanyang University (HYUH IRB 2013-06-012 and 2017-01-043).

Availability of data and materials

The transcriptome analyses performed in iMGs and brain tissue are available upon request.

Conflicts of interest

All authors declare that they have no competing interests.

Funding

This study was supported by a grant (NRF-2018M3C7A1056512) from the Brain Research Program of the National Research Foundation (NRF) funded by the Ministry of Science & ICT, and also supported by the Korea Health Technology R&D Project through the Korea Health Industry, Development Institute (KHIDI), funded by the Ministry of Health & Welfare, Republic of Korea (HI16C2131).

Authors' contributions

MY. N, and MS. K. contributed to the conception and design of the experiments, interpreted the data, and wrote the manuscript. KW. O. and JS. P. contributed to the clinical data. CS. K. and YE. K. performed the genetic analysis. M. N. analyzed the RNA transcripts. JS. B. and HK. J. contributed to drafting of the text.

SH. K. supervised the experiments and wrote the manuscript. All authors critically revised the manuscript and approved the final article.

Acknowledgments

We thank the staff from the Department of Neurology, College of Medicine, Hanyang University and the patients for participating in this study. We also thank all group members of the S.H.K lab for their helpful discussions.

References

1. Mitchell JD, Borasio GD: **Amyotrophic lateral sclerosis.** *Lancet* 2007, **369:**2031-2041.
2. Ilieva H, Polymenidou M, Cleveland DW: **Non-cell autonomous toxicity in neurodegenerative disorders: ALS and beyond.** *J Cell Biol* 2009, **187:**761-772.
3. Rudnick ND, Griffey CJ, Guarnieri P, Gerbino V, Wang X, Piersaint JA, Tapia JC, Rich MM, Maniatis T: **Distinct roles for motor neuron autophagy early and late in the SOD1(G93A) mouse model of ALS.** *Proc Natl Acad Sci U S A* 2017, **114:**E8294-E8303.
4. Beers DR, Henkel JS, Zhao W, Wang J, Appel SH: **CD4+ T cells support glial neuroprotection, slow disease progression, and modify glial morphology in an animal model of inherited ALS.** *Proc Natl Acad Sci U S A* 2008, **105:**15558-15563.
5. Spiller KJ, Restrepo CR, Khan T, Dominique MA, Fang TC, Canter RG, Roberts CJ, Miller KR, Ransohoff RM, Trojanowski JQ, Lee VM: **Microglia-mediated recovery from ALS-relevant motor neuron degeneration in a mouse model of TDP-43 proteinopathy.** *Nat Neurosci* 2018, **21:**329-340.
6. Svahn AJ, Don EK, Badrock AP, Cole NJ, Graeber MB, Yerbury JJ, Chung R, Morsch M: **Nucleo-cytoplasmic transport of TDP-43 studied in real time: impaired microglia function leads to axonal spreading of TDP-43 in degenerating motor neurons.** *Acta Neuropathol* 2018, **136:**445-459.
7. Gordon PH, Moore DH, Miller RG, Florence JM, Verheijde JL, Doorish C, Hilton JF, Spitalny GM, MacArthur RB, Mitsumoto H, et al: **Efficacy of minocycline in patients with amyotrophic lateral sclerosis: a phase III randomised trial.** *Lancet Neurol* 2007, **6:**1045-1053.
8. Cudkowicz ME, Shefner JM, Schoenfeld DA, Zhang H, Andreasson KI, Rothstein JD, Drachman DB: **Trial of celecoxib in amyotrophic lateral sclerosis.** *Ann Neurol* 2006, **60:**22-31.
9. Masuda T, Sankowski R, Staszewski O, Bottcher C, Amann L, Sagar, Scheiwe C, Nessler S, Kunz P, van Loo G, et al: **Spatial and temporal heterogeneity of mouse and human microglia at single-cell resolution.** *Nature* 2019, **566:**388-392.
10. Boillee S, Yamanaka K, Lobsiger CS, Copeland NG, Jenkins NA, Kassiotis G, Kollias G, Cleveland DW: **Onset and progression in inherited ALS determined by motor neurons and microglia.** *Science* 2006, **312:**1389-1392.
11. Nagai M, Re DB, Nagata T, Chalazonitis A, Jessell TM, Wichterle H, Przedborski S: **Astrocytes expressing ALS-linked mutated SOD1 release factors selectively toxic to motor neurons.** *Nat Neurosci*

2007, **10:**615-622.

12. Beers DR, Appel SH: **Immune dysregulation in amyotrophic lateral sclerosis: mechanisms and emerging therapies.** *Lancet Neurol* 2019, **18:**211-220.
13. Zondler L, Muller K, Khalaji S, Bliederhauser C, Ruf WP, Grozdanov V, Thiemann M, Fundel-Clemes K, Freischmidt A, Holzmann K, et al: **Peripheral monocytes are functionally altered and invade the CNS in ALS patients.** *Acta Neuropathol* 2016, **132:**391-411.
14. Butovsky O, Siddiqui S, Gabriely G, Lanser AJ, Dake B, Murugaiyan G, Doykan CE, Wu PM, Gali RR, Iyer LK, et al: **Modulating inflammatory monocytes with a unique microRNA gene signature ameliorates murine ALS.** *J Clin Invest* 2012, **122:**3063-3087.
15. Butovsky O, Jedrychowski MP, Cialic R, Krasemann S, Murugaiyan G, Fanek Z, Greco DJ, Wu PM, Doykan CE, Kiner O, et al: **Targeting miR-155 restores abnormal microglia and attenuates disease in SOD1 mice.** *Ann Neurol* 2015, **77:**75-99.
16. Krasemann S, Madore C, Cialic R, Baufeld C, Calcagno N, El Fatimy R, Beckers L, O'Loughlin E, Xu Y, Fanek Z, et al: **The TREM2-APOE Pathway Drives the Transcriptional Phenotype of Dysfunctional Microglia in Neurodegenerative Diseases.** *Immunity* 2017, **47:**566-581 e569.
17. Keren-Shaul H, Spinrad A, Weiner A, Matcovitch-Natan O, Dvir-Szternfeld R, Ulland TK, David E, Baruch K, Lara-Astaiso D, Toth B, et al: **A Unique Microglia Type Associated with Restricting Development of Alzheimer's Disease.** *Cell* 2017, **169:**1276-1290 e1217.
18. Rangaraju S, Dammer EB, Raza SA, Rathakrishnan P, Xiao H, Gao T, Duong DM, Pennington MW, Lah JJ, Seyfried NT, Levey AI: **Identification and therapeutic modulation of a pro-inflammatory subset of disease-associated-microglia in Alzheimer's disease.** *Mol Neurodegener* 2018, **13:**24.
19. Abud EM, Ramirez RN, Martinez ES, Healy LM, Nguyen CHH, Newman SA, Yeromin AV, Scarfone VM, Marsh SE, Fimbres C, et al: **iPSC-Derived Human Microglia-like Cells to Study Neurological Diseases.** *Neuron* 2017, **94:**278-293 e279.
20. Pandya H, Shen MJ, Ichikawa DM, Sedlock AB, Choi Y, Johnson KR, Kim G, Brown MA, Elkahloun AG, Maric D, et al: **Differentiation of human and murine induced pluripotent stem cells to microglia-like cells.** *Nat Neurosci* 2017, **20:**753-759.
21. Muffat J, Li Y, Yuan B, Mitalipova M, Omer A, Corcoran S, Bakiasi G, Tsai LH, Aubourg P, Ransohoff RM, Jaenisch R: **Efficient derivation of microglia-like cells from human pluripotent stem cells.** *Nat Med* 2016, **22:**1358-1367.
22. Mertens J, Paquola ACM, Ku M, Hatch E, Bohnke L, Ladjevardi S, McGrath S, Campbell B, Lee H, Herdy JR, et al: **Directly Reprogrammed Human Neurons Retain Aging-Associated Transcriptomic Signatures and Reveal Age-Related Nucleocytoplasmic Defects.** *Cell Stem Cell* 2015, **17:**705-718.
23. Ryan KJ, White CC, Patel K, Xu J, Olah M, Replogle JM, Frangieh M, Cimpean M, Winn P, McHenry A, et al: **A human microglia-like cellular model for assessing the effects of neurodegenerative disease gene variants.** *Sci Transl Med* 2017, **9**.
24. Ohgidani M, Kato TA, Kanba S: **Introducing directly induced microglia-like (iMG) cells from fresh human monocytes: a novel translational research tool for psychiatric disorders.** *Front Cell Neurosci*

2015, **9:**184.

25. Li Q, Barres BA: **Microglia and macrophages in brain homeostasis and disease.** *Nat Rev Immunol* 2018, **18:**225-242.
26. Sellgren CM, Sheridan SD, Gracias J, Xuan D, Fu T, Perlis RH: **Patient-specific models of microglia-mediated engulfment of synapses and neural progenitors.** *Mol Psychiatry* 2017, **22:**170-177.
27. Ohgidani M, Kato TA, Setoyama D, Sagata N, Hashimoto R, Shigenobu K, Yoshida T, Hayakawa K, Shimokawa N, Miura D, et al: **Direct induction of ramified microglia-like cells from human monocytes: dynamic microglial dysfunction in Nasu-Hakola disease.** *Sci Rep* 2014, **4:**4957.
28. Ikawa D, Makinodan M, Iwata K, Ohgidani M, Kato TA, Yamashita Y, Yamamuro K, Kimoto S, Toritsuka M, Yamauchi T, et al: **Microglia-derived neuregulin expression in psychiatric disorders.** *Brain Behav Immun* 2017, **61:**375-385.
29. Brooks BR: **El Escorial World Federation of Neurology criteria for the diagnosis of amyotrophic lateral sclerosis. Subcommittee on Motor Neuron Diseases/Amyotrophic Lateral Sclerosis of the World Federation of Neurology Research Group on Neuromuscular Diseases and the El Escorial "Clinical limits of amyotrophic lateral sclerosis" workshop contributors.** *Journal of the neurological sciences* 1994, **124 Suppl:**96-107.
30. Labra J, Menon P, Byth K, Morrison S, Vucic S: **Rate of disease progression: a prognostic biomarker in ALS.** *J Neurol Neurosurg Psychiatry* 2016, **87:**628-632.
31. Kwon MS, Noh MY, Oh KW, Cho KA, Kang BY, Kim KS, Kim YS, Kim SH: **The immunomodulatory effects of human mesenchymal stem cells on peripheral blood mononuclear cells in ALS patients.** *J Neurochem* 2014, **131:**206-218.
32. Melief J, Koning N, Schuurman KG, Van De Garde MD, Smolders J, Hoek RM, Van Eijk M, Hamann J, Huitinga I: **Phenotyping primary human microglia: tight regulation of LPS responsiveness.** *Glia* 2012, **60:**1506-1517.
33. Erny D, Hrabe de Angelis AL, Jaitin D, Wieghofer P, Staszewski O, David E, Keren-Shaul H, Mahlakoiv T, Jakobshagen K, Buch T, et al: **Host microbiota constantly control maturation and function of microglia in the CNS.** *Nat Neurosci* 2015, **18:**965-977.
34. Lian H, Roy E, Zheng H: **Microglial Phagocytosis Assay.** *Bio Protoc* 2016, **6**.
35. Lukinavicius G, Reymond L, D'Este E, Masharina A, Gottfert F, Ta H, Guther A, Fournier M, Rizzo S, Waldmann H, et al: **Fluorogenic probes for live-cell imaging of the cytoskeleton.** *Nat Methods* 2014, **11:**731-733.
36. Mizee MR, Miedema SS, van der Poel M, Adelia, Schuurman KG, van Strien ME, Melief J, Smolders J, Hendrickx DA, Heutinck KM, et al: **Isolation of primary microglia from the human post-mortem brain: effects of ante- and post-mortem variables.** *Acta Neuropathol Commun* 2017, **5:**16.
37. Langmead B, Salzberg SL: **Fast gapped-read alignment with Bowtie 2.** *Nat Methods* 2012, **9:**357-359.
38. Gentleman RC, Carey VJ, Bates DM, Bolstad B, Dettling M, Dudoit S, Ellis B, Gautier L, Ge Y, Gentry J, et al: **Bioconductor: open software development for computational biology and bioinformatics.** *Genome Biol* 2004, **5:**R80.

39. Galatro TF, Holtman IR, Lerario AM, Vainchtein ID, Brouwer N, Sola PR, Veras MM, Pereira TF, Leite REP, Moller T, et al: **Transcriptomic analysis of purified human cortical microglia reveals age-associated changes.** *Nat Neurosci* 2017, **20:**1162-1171.
40. Butovsky O, Jedrychowski MP, Moore CS, Cialic R, Lanser AJ, Gabriely G, Koeglsperger T, Dake B, Wu PM, Doykan CE, et al: **Identification of a unique TGF-beta-dependent molecular and functional signature in microglia.** *Nat Neurosci* 2014, **17:**131-143.
41. Deczkowska A, Amit I, Schwartz M: **Microglial immune checkpoint mechanisms.** *Nat Neurosci* 2018, **21:**779-786.
42. Li W: **Phagocyte dysfunction, tissue aging and degeneration.** *Ageing Res Rev* 2013, **12:**1005-1012.
43. Weiner OD, Rentel MC, Ott A, Brown GE, Jedrychowski M, Yaffe MB, Gygi SP, Cantley LC, Bourne HR, Kirschner MW: **Hem-1 complexes are essential for Rac activation, actin polymerization, and myosin regulation during neutrophil chemotaxis.** *PLoS Biol* 2006, **4:**e38.
44. Chen Z, Borek D, Padrick SB, Gomez TS, Metlagel Z, Ismail AM, Umetani J, Billadeau DD, Otwinowski Z, Rosen MK: **Structure and control of the actin regulatory WAVE complex.** *Nature* 2010, **468:**533-538.
45. Park H, Chan MM, Iritani BM: **Hem-1: putting the "WAVE" into actin polymerization during an immune response.** *FEBS Lett* 2010, **584:**4923-4932.
46. Haney MS, Bohlen CJ, Morgens DW, Ousey JA, Barkal AA, Tsui CK, Ego BK, Levin R, Kamber RA, Collins H, et al: **Identification of phagocytosis regulators using magnetic genome-wide CRISPR screens.** *Nat Genet* 2018, **50:**1716-1727.
47. Park H, Staehling-Hampton K, Appleby MW, Brunkow ME, Habib T, Zhang Y, Ramsdell F, Liggitt HD, Freie B, Tsang M, et al: **A point mutation in the murine Hem1 gene reveals an essential role for Hematopoietic protein 1 in lymphopoiesis and innate immunity.** *J Exp Med* 2008, **205:**2899-2913.
48. Afzal TA, Luong LA, Chen D, Zhang C, Yang F, Chen Q, An W, Wilkes E, Yashiro K, Cutillas PR, et al: **NCK Associated Protein 1 Modulated by miRNA-214 Determines Vascular Smooth Muscle Cell Migration, Proliferation, and Neointima Hyperplasia.** *J Am Heart Assoc* 2016, **5**.
49. Xiao CZ, Wei W, Guo ZX, Zhang MY, Zhang YF, Wang JH, Shi M, Wang HY, Guo RP: **MicroRNA-34c-3p promotes cell proliferation and invasion in hepatocellular carcinoma by regulation of NCKAP1 expression.** *J Cancer Res Clin Oncol* 2017, **143:**263-273.
50. Zhao W, Beers DR, Hooten KG, Sieglaff DH, Zhang A, Kalyana-Sundaram S, Traini CM, Halsey WS, Hughes AM, Sathe GM, et al: **Characterization of Gene Expression Phenotype in Amyotrophic Lateral Sclerosis Monocytes.** *JAMA Neurol* 2017.
51. Kettenmann H, Hanisch UK, Noda M, Verkhratsky A: **Physiology of microglia.** *Physiol Rev* 2011, **91:**461-553.
52. Ummenthum K, Peferoen LA, Finardi A, Baker D, Pryce G, Mantovani A, Bsibsi M, Bottazzi B, Peferoen-Baert R, van der Valk P, et al: **Pentraxin-3 is upregulated in the central nervous system during MS and EAE, but does not modulate experimental neurological disease.** *Eur J Immunol* 2016, **46:**701-711.
53. Guerreiro R, Wojtas A, Bras J, Carrasquillo M, Rogaeva E, Majounie E, Cruchaga C, Sassi C, Kauwe JS, Younkin S, et al: **TREM2 variants in Alzheimer's disease.** *N Engl J Med* 2013, **368:**117-127.

54. Colonna M, Wang Y: **TREM2 variants: new keys to decipher Alzheimer disease pathogenesis.** *Nat Rev Neurosci* 2016, **17:**201-207.

55. Rayaprolu S, Mullen B, Baker M, Lynch T, Finger E, Seeley WW, Hatanpaa KJ, Lomen-Hoerth C, Kertesz A, Bigio EH, et al: **TREM2 in neurodegeneration: evidence for association of the p.R47H variant with frontotemporal dementia and Parkinson's disease.** *Mol Neurodegener* 2013, **8:**19.

56. Cady J, Koval ED, Benitez BA, Zaidman C, Jockel-Balsarotti J, Allred P, Baloh RH, Ravits J, Simpson E, Appel SH, et al: **TREM2 variant p.R47H as a risk factor for sporadic amyotrophic lateral sclerosis.** *JAMA Neurol* 2014, **71:**449-453.

57. Suzuki T, Nishiyama K, Yamamoto A, Inazawa J, Iwaki T, Yamada T, Kanazawa I, Sakaki Y: **Molecular cloning of a novel apoptosis-related gene, human Nap1 (NCKAP1), and its possible relation to Alzheimer disease.** *Genomics* 2000, **63:**246-254.

58. Yokota Y, Ring C, Cheung R, Pevny L, Anton ES: **Nap1-regulated neuronal cytoskeletal dynamics is essential for the final differentiation of neurons in cerebral cortex.** *Neuron* 2007, **54:**429-445.

59. Beers DR, Henkel JS, Xiao Q, Zhao W, Wang J, Yen AA, Siklos L, McKercher SR, Appel SH: **Wild-type microglia extend survival in PU.1 knockout mice with familial amyotrophic lateral sclerosis.** *Proc Natl Acad Sci U S A* 2006, **103:**16021-16026.

60. Luo XG, Chen SD: **The changing phenotype of microglia from homeostasis to disease.** *Transl Neurodegener* 2012, **1:**9.

61. Streit WJ, Xue QS, Tischer J, Bechmann I: **Microglial pathology.** *Acta Neuropathol Commun* 2014, **2:**142.

62. Norden DM, Godbout JP: **Review: microglia of the aged brain: primed to be activated and resistant to regulation.** *Neuropathol Appl Neurobiol* 2013, **39:**19-34.

63. Deczkowska A, Keren-Shaul H, Weiner A, Colonna M, Schwartz M, Amit I: **Disease-Associated Microglia: A Universal Immune Sensor of Neurodegeneration.** *Cell* 2018, **173:**1073-1081.

64. Sousa C, Golebiewska A, Poovathingal SK, Kaoma T, Pires-Afonso Y, Martina S, Coowar D, Azuaje F, Skupin A, Balling R, et al: **Single-cell transcriptomics reveals distinct inflammation-induced microglia signatures.** *EMBO Rep* 2018, **19**.

65. Parisi C, Arisi I, D'Ambrosi N, Storti AE, Brandi R, D'Onofrio M, Volonte C: **Dysregulated microRNAs in amyotrophic lateral sclerosis microglia modulate genes linked to neuroinflammation.** *Cell Death Dis* 2013, **4:**e959.

66. Ricci C, Marzocchi C, Battistini S: **MicroRNAs as Biomarkers in Amyotrophic Lateral Sclerosis.** *Cells* 2018, **7**.

67. Waller R, Goodall EF, Milo M, Cooper-Knock J, Da Costa M, Hobson E, Kazoka M, Wollff H, Heath PR, Shaw PJ, Kirby J: **Serum miRNAs miR-206, 143-3p and 374b-5p as potential biomarkers for amyotrophic lateral sclerosis (ALS).** *Neurobiol Aging* 2017, **55:**123-131.

68. Polytarchou C, Hommes DW, Palumbo T, Hatziapostolou M, Koutsioumpa M, Koukos G, van der Meulen-de Jong AE, Oikonomopoulos A, van Deen WK, Vorvis C, et al: **MicroRNA214 Is Associated**

With Progression of Ulcerative Colitis, and Inhibition Reduces Development of Colitis and Colitis-Associated Cancer in Mice. *Gastroenterology* 2015, **149:**981-992 e911.

69. Min SW, Sohn PD, Cho SH, Swanson RA, Gan L: **Sirtuins in neurodegenerative diseases: an update on potential mechanisms.** *Front Aging Neurosci* 2013, **5:**53.
70. Marro S, Pang ZP, Yang N, Tsai MC, Qu K, Chang HY, Sudhof TC, Wernig M: **Direct lineage conversion of terminally differentiated hepatocytes to functional neurons.** *Cell Stem Cell* 2011, **9:**374-382.
71. Tang Y, Liu ML, Zang T, Zhang CL: **Direct Reprogramming Rather than iPSC-Based Reprogramming Maintains Aging Hallmarks in Human Motor Neurons.** *Front Mol Neurosci* 2017, **10:**359.
72. Lemaire I, Falzoni S, Zhang B, Pellegatti P, Di Virgilio F: **The P2X7 receptor and Pannexin-1 are both required for the promotion of multinucleated macrophages by the inflammatory cytokine GM-CSF.** *J Immunol* 2011, **187:**3878-3887.
73. Fleetwood AJ, Lawrence T, Hamilton JA, Cook AD: **Granulocyte-macrophage colony-stimulating factor (CSF) and macrophage CSF-dependent macrophage phenotypes display differences in cytokine profiles and transcription factor activities: implications for CSF blockade in inflammation.** *J Immunol* 2007, **178:**5245-5252.
74. Ginhoux F, Greter M, Leboeuf M, Nandi S, See P, Gokhan S, Mehler MF, Conway SJ, Ng LG, Stanley ER, et al: **Fate mapping analysis reveals that adult microglia derive from primitive macrophages.** *Science* 2010, **330:**841-845.

Additional Files

Additional file 1: Table S1. Demographics of the enrolled participants, including healthy controls and ALS patients with slow and rapid clinical progression.

Additional file 2: Figure S1. Flow chart of the overall experiment.

Additional file 3: Table S2. Genetic panels related to ALS, FTD, and other types of dementia.

Additional file 4: Figure S2. Morphology of iMGs according to time in culture.

Additional file 5: Table S3. List of 705 shared genes in iMGs and Brain-MG according to whole-transcriptome differential gene expression analysis.

Additional file 5: Table S4. GO analysis and KEGG pathways in 705 genes shared by iMGs and brain-MG.

Additional file 5: Table S5. GO analysis of 861 genes shared by ALS-iMGs and HC-iMGs.

Additional file 5: Table S6. List of 2,559 shared genes in ALS(R)-iMGs and ALS(S)-iMGs according to whole-transcriptome differential gene expression.

Additional file 5: Table S7. GO analysis and KEGG pathways in 2,559 genes significantly altered in ALS(R)-iMGs compared with ALS(S)-iMGs.

Additional file 6: Figure S3. Defective phagocytic function of ALS(R)-iMGs in groups #1 and #2.

Additional file 7: Figure S4. *NCKAP1*, *miRNA-214*, and *miRNA-34* expression in iMGs.

Additional file 8: Figure S5. Efficacy of *NCKAP1* knockdown and involvement of NCKAP1 in actin structure formation.

Additional file 9: Video S1. Live image of phagocytosis of a latex bead in ALS(S)-iMGs.

Additional file 10: Video S2. Live image of phagocytosis in ALS(S)-iMGs after *NCKAP1* knockdown.

Additional file 11: Video S3. Live image of phagocytosis in ALS(R)-iMGs.

Additional file 12: Video S4. Live image of phagocytosis in ALS(R)-iMGs after *NCKAP1* overexpression.

Additional file 13: Figure S6. The culture environment used for iMG generation [+GM-CSF, IL-34 (21d)] can mirror differential cytokine expression in HC-iMGs and ALS-iMGs without phenotypic reset.

Additional file 14: Figure S7. The culture environment used for iMG generation can mirror sufficiently differential cytokine expression in ALS(S)-iMGs and ALS(R)-iMGs.

Additional file 15: Figure S8. *Post-hoc* analysis of plasma cytokine levels in HCs, slowly progressing ALS, and rapidly progressing ALS patients.

Figures

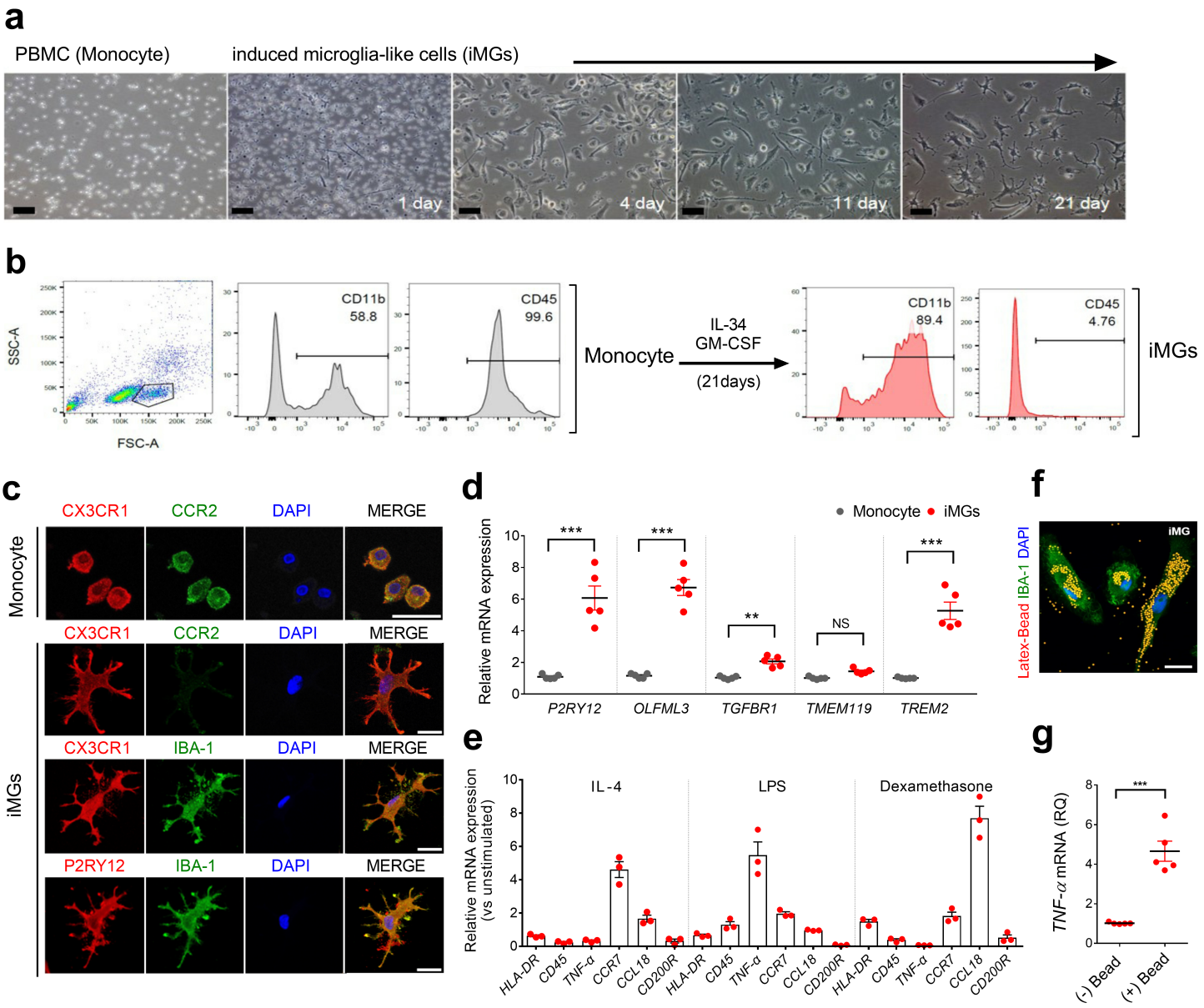

Figure 1

Characterization of iMGs for subsequent experiments using the iMGs model. A Representative images of monocytes and iMGs in different stages, taken on days 1, 4, 11, and 21. iMGs generated from monocytes treated with GM-CSF and IL-34 for 21 days showing similar morphology to ramified microglia. Scale bar: 100 µm. b In flow cytometry, most iMGs showed high CD11b and low CD45 expression on day 21. c iMGs expressed CX3CR1 (green) and the specific microglial markers P2RY12 (red) and IBA-1 (green), but not CCR2 (green), a marker of monocytes. DAPI (blue) was used to visualize nuclei. The figure is representative of several replicates of independent experiments (n = 6). Scale bar: 25 µm. d Microglial signature gene expression profiles (P2RY12, OLFML3, TGFBR1, TMEM119, and TREM2) of iMGs analyzed by qRT-PCR. Fold changes in mRNA expression compared to monocytes. Each dot represents data from one individual's HC-iMGs and monocytes (n = 5 in group #1) e Cytokine expression profiles for iMGs stimulated with LPS, dexamethasone, or IL-4 analyzed by qRT-PCR. Each dot represents data from

an individual's HC-iMGs (n = 3 in group #1). f Phagocytic activity of iMGs (IBA-1: green) incubated with fluorescent latex beads (red) for 24 h. DAPI (blue) was used to visualize nuclei. The figure is representative of several independent experiments (n = 5). Scale bar: 25 µm. g After phagocytosis for 72 h, TNF-α mRNA expression in iMGs was significantly higher than that in controls (vs. without bead). Each dot represents data from an individual's HC-iMGs and monocytes (n = 5 in group #1). In (d–g), data are presented as mean ± SEM. **p < 0.01, ***p < 0.001, NS: not significant (Student's t-test or one-way ANOVA).

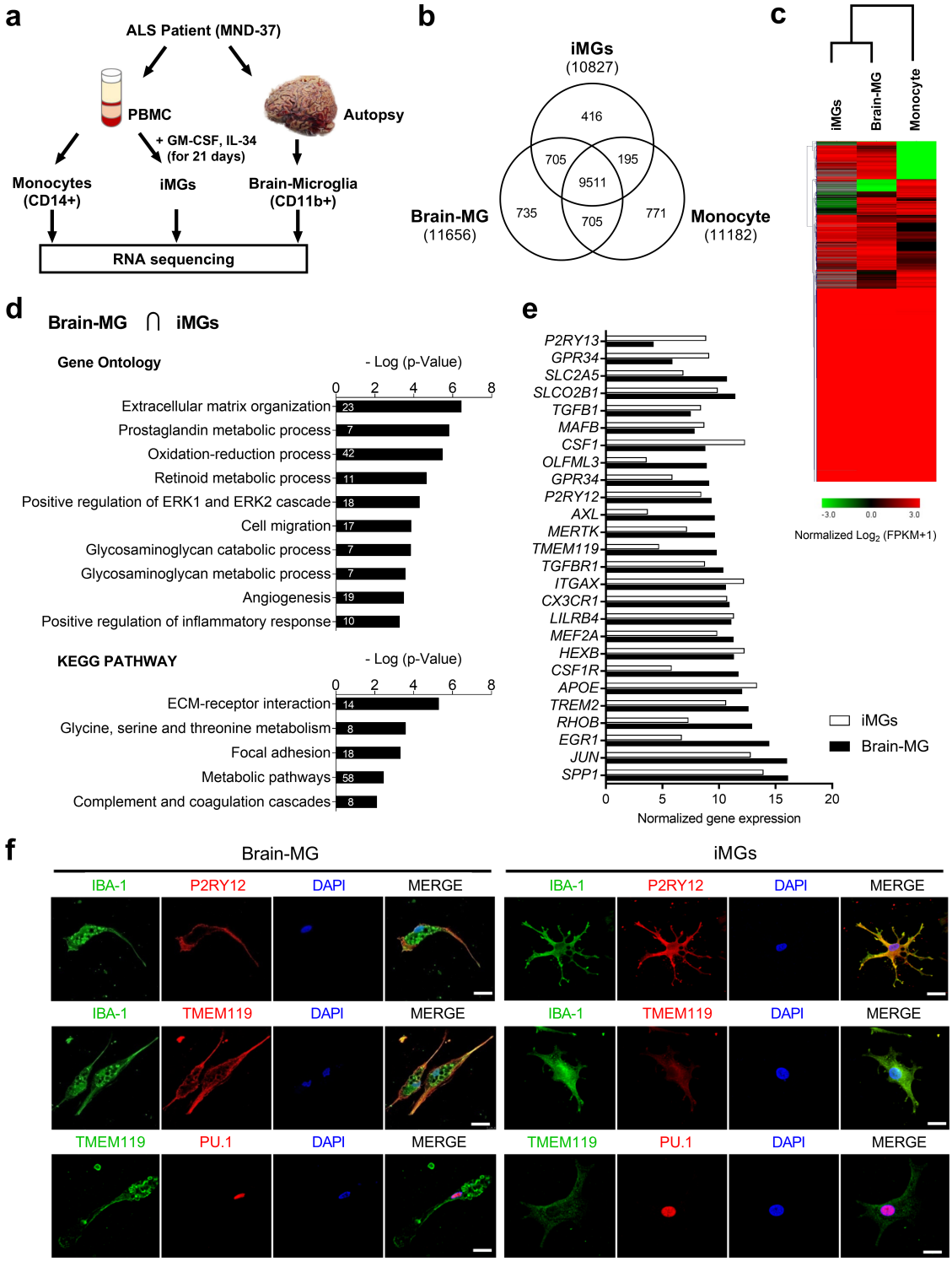

Figure 2

Transcriptome comparison between iMGs and brain microglia obtained simultaneously from a single ALS patient. a Schematic representation of the experimental procedure used to compare iMGs with brain microglia (brain-MG) and monocytes in a ALS patient. b Venn diagram showing unique and intersecting genes (13,038) that are differentially expressed (DE) in monocytes, iMGs, and brain-MG according to RNA-seq (Fold Change > |3|). c Heatmap of DE genes from gene transcriptome comparisons between monocytes, iMGs, and brain-MG. A pseudo-count was used to obtain FPKM values (FPKM +1), log2-transformed, and each gene was normalized in its respective row (n = 13,038). d GO analysis of ten significant pathway modules and five KEGG pathway modules in the 705 genes shared between iMGs and brain-MG. The number within each bar indicates the number of genes in the database for the specified term. e Bar graphs of microglial-specific or -enriched genes measured in iMGs and brain-MG as [log2 (FPKM +1)] presented as mean ± SEM. f Immunocytochemical staining of IBA-1, P2RY12, TMEM119, and PU.1. DAPI was used to visualize nuclei. The figure is representative of independent experiments performed in replicates (n = 10). Scale bar: 25 μm.

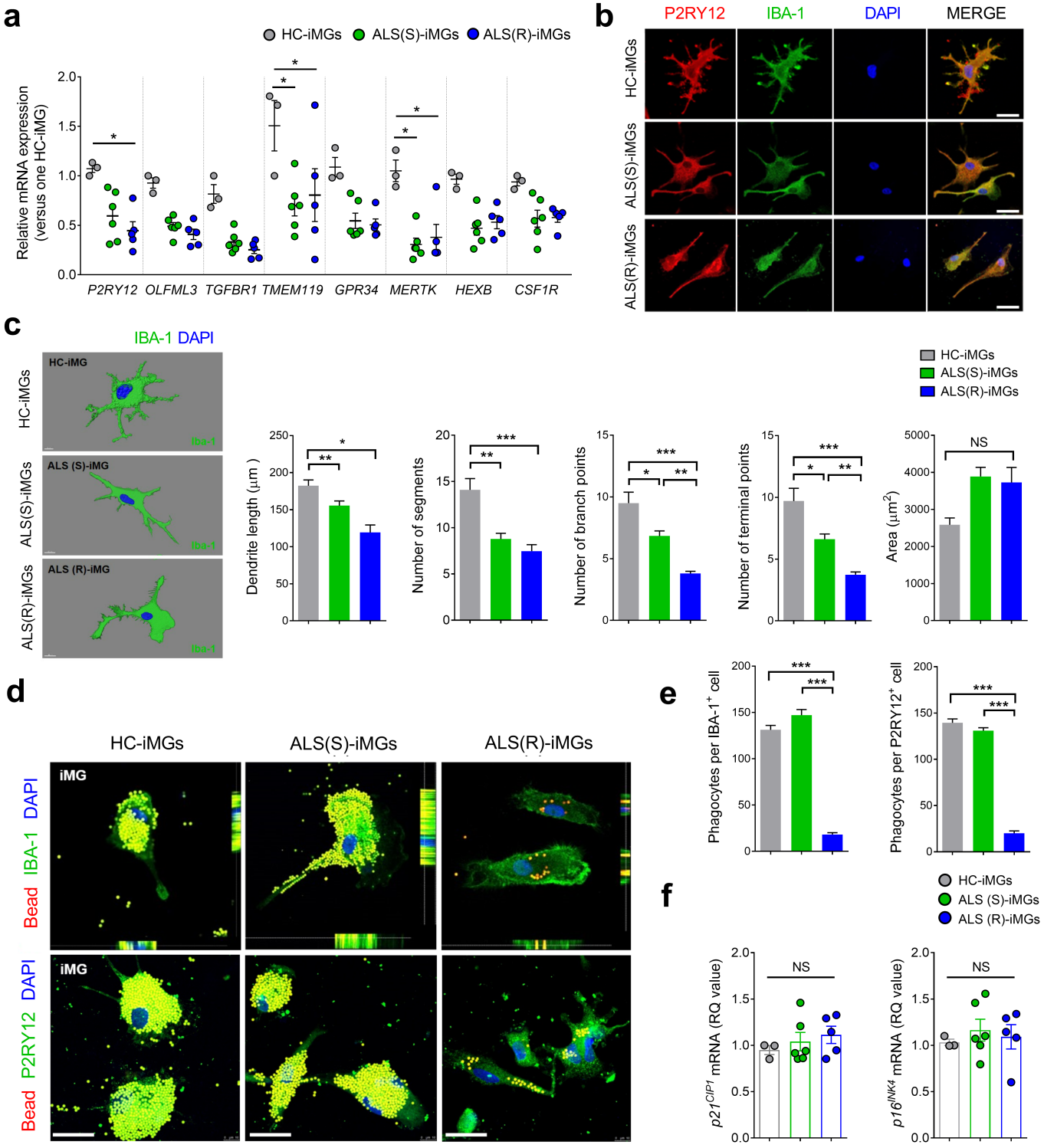

Figure 3

Dystrophic morphology and defective phagocytic function of ALS(R)-iMGs compared to ALS(S)-iMGs. a Expression pattern of the main homeostatic microglial signature genes in both groups of ALS-iMGs and HC-iMGs. Each dot represents data from individual-subject-derived iMGs (HC-iMGs: n = 3; ALS(S)-iMGs: n = 6; ALS(R)-iMGs: n = 5, group #1). *p < 0.05 compared to HC-iMGs. b Immunocytochemcial staining of the three groups of iMGs. iMGs with antibodies against P2RY12 (red) and IBA-1 (green). DAPI was used

to visualize nuclei. The figure is representative of three independent experiments (n = 10). Scale bar: 25 μm. c Imaris-based morphometric analysis comparing the three groups' iMGs (IBA-1; green). Each column represents the mean of each group's iMGs with at least 10 randomly selected cells per subject-derived iMGs. d, e Comparative images showing phagocytic activity in the three groups' iMGs. iMGs from each group were incubated with latex beads for 24 h and the number of phagocytized beads per IBA-1-positive cell or P2RY12-positive cell was counted using Image J software. IBA-1 and P2RY12 were used as iMG markers (green) (d). The figure represents several independent experiments conducted in replicates (n = 3). Scale bar: 25 μm. Each data point represents the mean of each group's iMGs with at least 10 cells per subject-derived iMGs (e). f qRT-PCR analysis of p21 and p16 expression in the three groups' iMGs. Each data point represents individual-subject-derived iMGs (HC: n = 3; ALS(S)-iMGs: n = 6; ALS(R)-iMGs: n = 5, group #1). In (a, c, e, f), data are presented as mean ± SEM. *p < 0.05, **p < 0.01, ***p < 0.001, NS: not significant (one-way ANOVA).

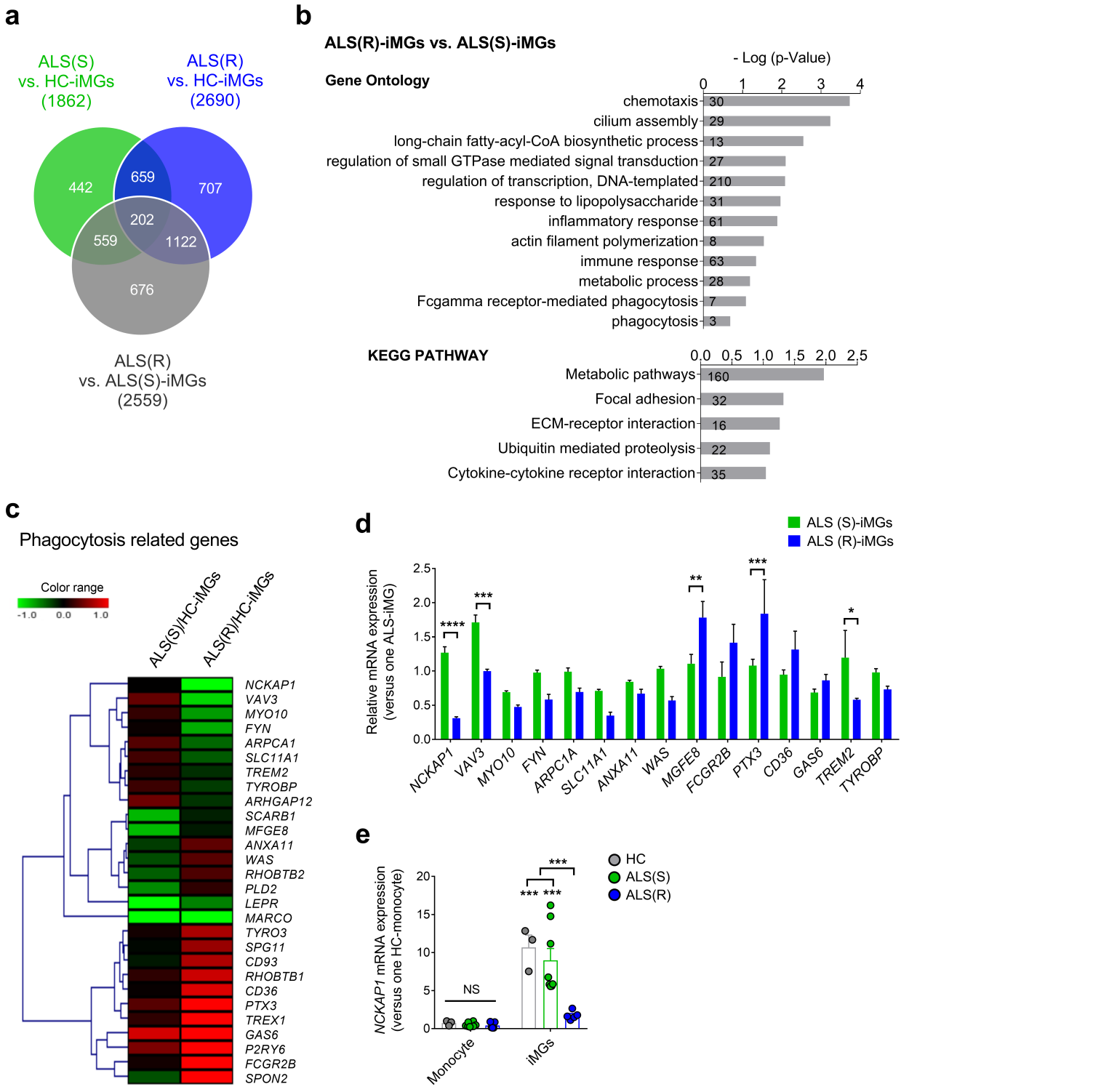

Figure 4

Transcriptome analysis showing that low NCKAP1 expression is associated with impaired phagocytic function in rapidly progressing ALS-iMGs. Transcriptome analysis of the three groups' iMGs (HC, ALS(S), and ALS(R)) generated from three HC, four ALS(S), and three ALS(R) patients (group #2). a Venn diagram illustrating the number of and overlap between transcripts that differed significantly in the three groups according to RNA-seq (Fold Change > |1.5|). b GO analysis of ten significant pathway modules and five

KEGG pathway modules from 2,559 transcripts that were significantly altered in ALS(R)-iMGs compared with ALS(S)-iMGs. The number within each bar indicates the number of genes in the database for the specified term. c Heatmap analysis focused on phagocytosis (GO:0006909) comparing differential gene expression in ALS(S)-iMGs and ALS(R)-iMGs compared with HC-iMGs (Fold Change > |1.5|) and phagocytosis-related genes, TREM2 and TYROBP. d The expression of phagocytosis-related genes obtained by RNA-seq (c) was re-analyzed by qRT-PCR of iMGs from “groups #1 and #2.” e qRT-PCR analysis of NCKAP1 expression in individual-subject-derived monocytes or iMGs from the three groups. The symbols represent individual-subject-derived monocytes or iMGs (HC: n = 3; ALS(S): n = 8; ALS(R): n = 5, from available samples from group #1 and #2). In (d-e), data are presented as mean ± SEM. *p < 0.05, **p < 0.01, ***p < 0.001, **** p<0.0001, NS: not significant (two-way ANOVA).

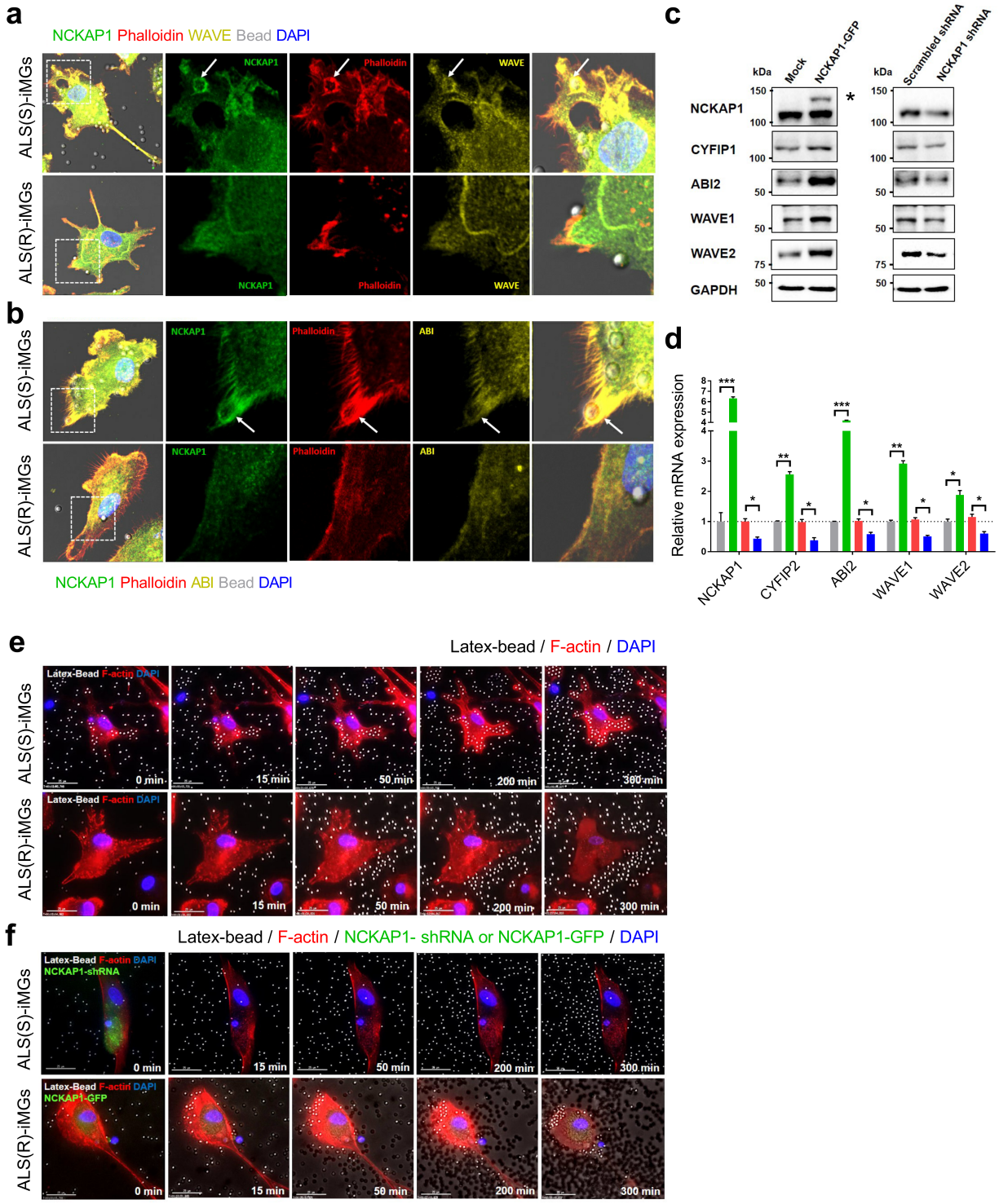

Figure 5

NCKAP1 regulates genes involved in actin polymerization and overexpression of NCKAP1 rescues defective phagocytic function in ALS(R)-iMGs. a, b Subcellular distribution of actin polymerization-related proteins and NCKAP1 during bead phagocytosis in both groups of ALS-iMGs (ALS(S)-iMGs and ALS(R)-iMGs). In ALS(S)-iMGs, WAVE (yellow; a) and ABI (yellow; b) were markedly accumulated at the phagocytic cups along with NCKAP1 (green) and phalloidin (red; F-actin marker). DAPI was used to

visualize nuclei. Arrows indicate phagocytic cups surrounding a bead. The figure is representative of independent experiments performed in replicates (n = 10). Scale bar: 25 μm. c, d Human NCKAP1 or shNCKAP1 was transfected into HeLa cells and changes in the expression of actin polymerization-related genes such as CYFIP1, ABI2, WAVE1, and WAVE2 were examined by Western blot. An empty shRNA vector was used as a control (scramble-shRNA). * represents NCKAP1-GFP (c). Quantification of expression level of each protein normalized to GAPDH and indicated as a percentage of vehicle control (n = 3). Data are presented as mean ± SEM. *p < 0.05, **p < 0.01, ***p < 0.001, NS: not significant (Two-way ANOVA) (d). e, f Snapshots of live cell imaging showing phagocytosis of latex beads in both groups of ALS-iMGs. Merged images of DIC (latex bead) and fluorescence images (F-actin: red; DAPI: blue). ALS(S)-iMGs (upper) showed normal phagocytic function, whereas ALS(R)-iMGs (lower) showed a marked impairment in phagocytosis (e). Latex bead phagocytosis in ALS(S)-iMGs transfected with shNCKAP1-GFP (upper) or ALS(R)-iMGs transfected with NCKAP1-GFP (lower) (f). The impaired phagocytic function in ALS(R)-iMGs was rescued by NCKAP1 overexpression. Representative frames from a time-lapse image series (0 - 5 h) are shown. The figure is representative of independent experiments performed in replicates (n = 10). Scale bar: 25 μm.

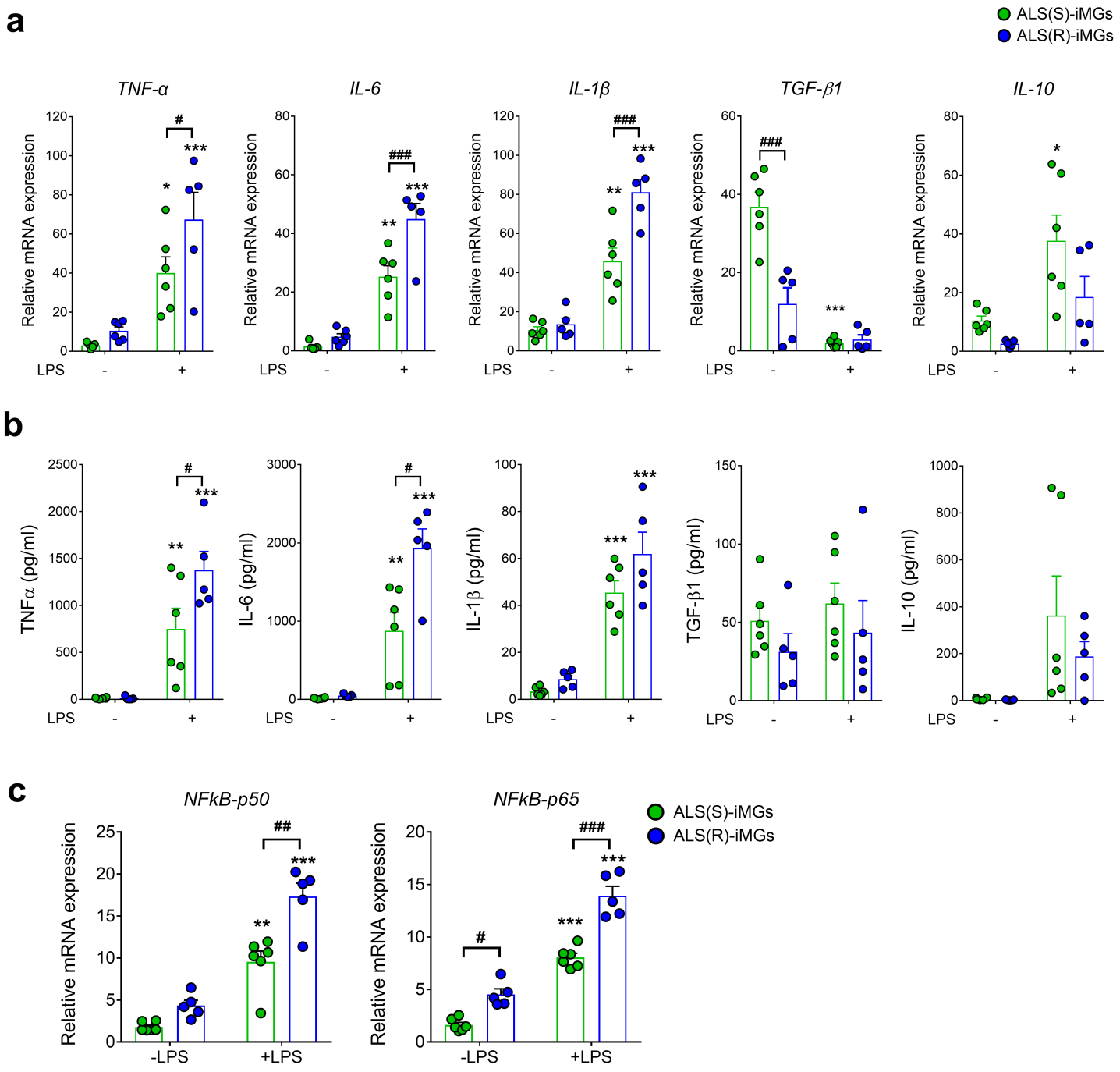

Figure 6

ALS(R)-iMGs exhibit an exaggerated pro-inflammatory response to LPS stimuli compared to ALS(S)-iMGs. a, b A comparison of cytokine profiles between ALS(S)-iMGs and ALS(R)-iMGs in the resting state or upon LPS stimulation (100 ng/ml), as evaluated by qRT-PCR (a) and ELISA (b). Each data point represents individual-subject-derived iMGs (ALS(S)-iMGs: n = 6; ALS(R)-iMGs: n = 5; from group #1). c NFκB-p50 and NFκB-p65 mRNA expression in ALS(S)-iMGs and ALS(R)-iMGs in the resting state or upon LPS stimulation. Each data point represents individual-subject-derived iMGs (ALS(S)-iMGs: n = 6; ALS(R)-iMGs: n = 5; from group #1). In (a-c), data are presented as mean ± SEM. *p < 0.05, **p < 0.01, ***p <

0.001 compared to no LPS treatment, #p < 0.05, ##p < 0.01, and ###p < 0.001 compared to ALS(S)-iMGs, NS: not significant in two-way ANOVA with Bonferroni's post hoc analysis).

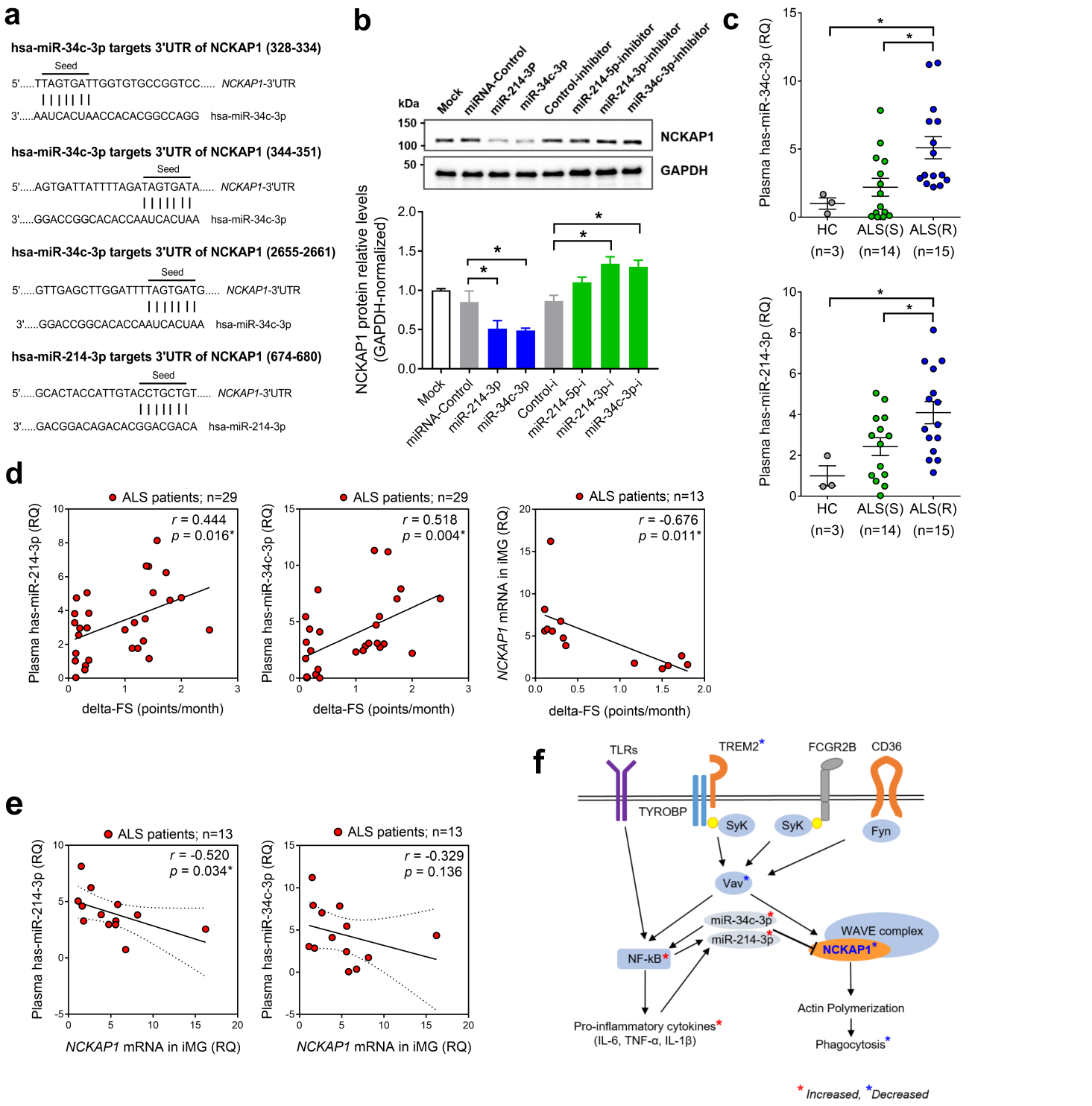

Figure 7

NCKAP1 and miRNA-214 are correlated with the rate of disease progression in ALS patients. a Alignment between NCKAP1 and miR-34c-3p or miR-214-3p, indicated by vertical bars (seed), predicted by bioinformatics sequence analysis. b NCKAP1 protein expression in HeLa cells transfected with miR-214-

3p/miR-34c-3p mimic, inhibitor, or a negative control. Quantification of NCKAP1 protein level was done via normalization to GAPDH (n = 3). c Relative expression of plasma miR-214-3p and miR-34c-3p in HCs, slowly progressing, and rapidly progressing ALS patients. Each data point represents one participant (HC: n = 3; ALS(S): n = 14; ALS(R): n = 15, all samples from groups #1, #2, #3). d Correlations of the relative expression of miR-214-3p in plasma, miR-34c-3p in plasma, and NCKAP1 in ALS-iMGs with rates of disease progression (delta-FS, points/month). Each data point represents one patient (miR-214-3p and miR-34c-3p in plasma: n = 29; NCKAP1 in ALS-iMGs: n = 13). p-values were obtained by Pearson correlation. e Correlations of the relative expression of miR-214-3p and miR-34c-3p in plasma with the relative expression of NCKAP1 in ALS-iMGs. Each data point represents one patient (n = 13). f Schematically summarized graphic pathway showing the possible microglial mechanism of rapidly progressing ALS. Briefly, actin polymerization could be altered by reduction of NCKAP1 expression, which might be associated with increased levels of miR-214-3p and miR-34c-3p within microglia, resulting in defective microglial phagocytosis. In (b-c), data are presented as mean ± SEM. *p < 0.05, **p < 0.01, ***p < 0.001, NS: not significant (one-way ANOVA).

Supplementary Files

This is a list of supplementary files associated with this preprint. Click to download.

- Additionalfile11VideoS3.avi
- Additionalfile10VideoS2.avi
- Additionalfile7FigureS4.tif
- Additionalfile6FigureS3.tif
- Additionalfile9VideoS1.avi
- Additionalfile1TableS1.pdf
- Additionalfile5TableS3S4S5S6S7.xlsx
- Additionalfile13FigureS6.tif
- Additionalfile14FigureS7.tif
- Additionalfile2FigureS1.tif
- Additionalfile4FigureS2.tif
- Additionalfile15FigureS8.tif
- Additionalfile8FigureS5.tif
- Additionalfile12VideoS4.avi
- Additionalfile3TableS2.pdf